



## CD47-SIRP $\alpha$ signaling-inspired engineered monocytes for preventing the progression of atherosclerotic plaques

Qing Xia <sup>a</sup>, Feila Liu <sup>a,\*</sup>, Yue Zhou <sup>a</sup>, Guanyuan Yang <sup>b</sup>, Fangzhou Li <sup>c</sup>, Tingting Liang <sup>a</sup>, Jun Liu <sup>a</sup>, Wanling Li <sup>a</sup>, Yaqing Huang <sup>a</sup>, Chuhong Zhu <sup>b,\*\*</sup>

<sup>a</sup> School of Pharmacy and Bioengineering, Chongqing University of Technology, Chongqing, 400054, China

<sup>b</sup> Department of Anatomy, State Key Laboratory of Trauma, Burn and Combined Injury, National and Regional Engineering Laboratory of Tissue Engineering, Third Military Medical University, Chongqing, 400038, China

<sup>c</sup> Institute of Biomedical Engineering, Chinese Academy of Medical Sciences and Peking Union Medical College, Tianjin, 300192, China

### ARTICLE INFO

**Keywords:**

Engineered monocytes  
CD47-SIRP $\alpha$   
Atherosclerosis  
Foam cell  
Cell therapy

### ABSTRACT

The accumulation of foam cells in the subendothelial space of the vascular wall to form plaques is the real cause of atherosclerotic lesions. Conventional interventions, such as statins and anti-cytokine or anti-inflammatory therapies, suffer problems in terms of their short therapeutic outcomes and potential disruption of the immune system. The development of more efficient therapeutics to restrict the initial progression of plaques appears to be crucial for treating and preventing atherosclerosis. Decreasing foam cell formation by reversing the excessive phagocytosis of modified low-density lipoprotein (LDL) in macrophages is highly desirable. Here, we developed a strategy based on engineered monocytes to dynamically regulate lipid uptake by macrophages inspired by a CD47-SIRP $\alpha$  signaling-induced defect in the phagocytosis of lesional macrophages at the advanced stage of AS. Briefly, a complex called CD47p-GQDs-miR223, which is designed to interact with SIRP $\alpha$ , was synthesized to remodel monocytes by decreasing the uptake of oxidized LDL through the activation of CD47-SIRP $\alpha$  signaling. After injection, these monocytes compete for recruitment to atherosclerotic plaques, release gene drugs and mediate anti-inflammatory phenotypic remodeling of the aboriginal macrophages, effectively inhibiting the development of foam cells. Our strategy provides a new therapeutic for preventing the progression of atherosclerosis.

### 1. Introduction

Atherosclerosis (AS) is considered a ‘ticking time bomb’ within the cardiovascular system and is characterized by the buildup of fatty deposits in the arteries. The accumulation of foam cells leads to the formation of fatty streaks, which can eventually develop into plaques that narrow and harden the arteries, increasing the risk of myocardial infarction and stroke and posing a serious threat to human life [1]. Foam cells primarily originate from monocytes after they penetrate the endothelial barrier and accumulate in the arterial intima media in response to the proinflammatory activation of endothelial cells (ECs) [2, 3]. These recruited monocytes subsequently differentiate into mature macrophages and accumulate lipids by actively ingesting modified low-density lipoprotein (LDL), along with artery-resident macrophages.

Essentially, macrophages can internalize and degrade

subendothelially retained lipoproteins in the early stages of atherosclerosis. However, due to the increased generation of oxidized low-density lipoprotein (ox-LDL), the macrophage expression of lectin-like ox-LDL receptor-1 (LOX-1) is significantly upregulated by stimulation with multiple factors, such as proinflammatory cytokines [4], lysophosphatidylcholine (a product of ox-LDL degradation) [5], and others. Elevated expression of LOX-1 in macrophages enhances their affinity for ox-LDL, resulting in increased lipid uptake. These macrophages are unable to efficiently remove excess lipids due to the inhibition of efflux pumps in the proinflammatory microenvironment [6], ultimately promoting excessive lipid uptake and impaired cholesterol outflow, leading to foam cell formation [7–9]. It is evident that lipid metabolism disorders in macrophages, mainly caused by the M1 phenotype [10–12], can be considered ‘excessive or aberrant phagocytosis’. Therefore, addressing the behavior of excessive phagocytosis of ox-LDL within

\* Corresponding author.

\*\* Corresponding author.

E-mail addresses: liufeila@cqut.edu.cn (F. Liu), zhuch99@tmmu.edu.cn (C. Zhu).

macrophages during lipid accumulation may be crucial for inhibiting foam cell formation. To tune the phagocytosis of ox-LDL by macrophages, the majority of related research has concentrated on the protein receptors that mediate macrophage phagocytosis, such as the mannose receptor [13], macrophage scavenger receptor A (SR-A) [14], and class B scavenger receptor CD36 [15,16]. These investigations of the scavenger receptor-mediated signaling pathway may lead to the identification of new therapeutic targets and novel strategies for treating AS. However, these receptors bind to a wide variety of ligands and participate in various biological processes, which may result in off-target side effects during delivery [17]. Therefore, the efficient uptake of ox-LDL by macrophages requires that the manageable and dynamic phagocytosis machinery operates optimally.

In atherosclerosis, nonapoptotic cells send a 'Don't eat me' signal [18,19], such as CD31, CD46, and CD47, to avoid efferocytosis when exposed to phagocytes. The most common ligand is CD47, which binds to the phagocytic inhibitory receptor signal regulatory protein  $\alpha$  (SIRP $\alpha$ ) on phagocytes to prevent phagocytosis [20–27]. In advanced plaques, increased CD47 hinders diseased cell clearance by lesional macrophages [28], whereas CD47 levels decrease in early plaques through a caspase-dependent process during apoptosis. Drawing inspiration from the phagocytosis inhibition facilitated by CD47, the CD47–SIRP $\alpha$  signaling pathway may provide exciting hints for controlling excessive phagocytosis in macrophages. Based on the above findings, we propose the following objectives: 1) replace some endogenous monocytes with substituted monocytes to decrease the amount of infiltrating pathological monocytes; 2) control phagocytosis by activating CD47–SIRP $\alpha$  signaling to decrease ox-LDL uptake by substituted monocytes in M1-polarizing atherosclerotic lesions; and 3) release drugs from the surface of substituted monocytes to induce anti-inflammatory phenotype remodeling of macrophages after CD47–SIRP $\alpha$  binding ends.

To accomplish these goals, we introduce a novel immune cell backpack approach utilizing CD47–SIRP $\alpha$  signal-mediated surface-engineered monocytes to target and treat atherosclerotic plaques in this research. In this distinctive engineered monocyte architecture, a disulfide bond was created between graphene quantum dots (GQDs) and microRNA223 (GQDs-S-S-miR223), followed by functionalization with a CD47-derived peptide (CD47p), ultimately resulting in a 'backpack' of CD47p-GQDs-miR223. The backpacks were later attached to the monocytes surface via CD47–SIRP $\alpha$  binding, transported into plaques by the natural trafficking of monocytes, where they were released to affect resident macrophages. GQDs were utilized as intermediate gene delivery vectors in our prior research for connecting biomacromolecules with gene drugs as well as facilitating the loading, protection and cellular internalization of gene drugs [29]. MiR223 can regulate the expression of numerous inflammation-related genes in monocytes and macrophages [30,31]. Engineered monocytes preserve their natural transport traits *in vivo*, hindering the infiltration of pathological monocytes through competitive recruitment. By dynamically activating and terminating 'do not-eat-me' signals, engineered monocytes can inhibit ox-LDL phagocytosis before the complete shedding of the backpack and regulate the plaque microenvironment from a proinflammatory to an anti-inflammatory state after CD47–SIRP $\alpha$  binding ends, ultimately leading to an enhanced plaque treatment effect. The successful construction of this innovative engineered monocyte therapy system offers a new strategy for clinical cellular immunotherapy for AS plaque treatment.

## 2. Materials and methods

### 2.1. Cell culture and animals

RAW264.7 cells were obtained from the cell bank of the American Type Culture Collection (ATCC, Shanghai Agency) and grown in complete DMEM supplemented with 10 % fetal calf serum (FCS) (Gibco),  $2 \times 10^{-3}$  M glutamine (HyClone), 100 U mL $^{-1}$  penicillin and 100  $\mu$ g mL $^{-1}$

streptomycin (HyClone). Male apolipoprotein E-deficient mice (*Apoe* $^{-/-}$ ) (18–23 g and 6 weeks old) were purchased from Vital River Experimental Animal Technology Co., Ltd. (Beijing, China). All mice were subjected to partial ligation of the RCCA and were fed a HFD (Research Diets D12108C, 1.25 % cholesterol). All procedures involving animals were reviewed and approved by the Institutional Animal Care and Use Committee (IACUC) of Chongqing University of Technology, Chongqing, China (No. 202321).

### 2.2. Preparation and characterization of engineered monocytes

The functionalization of the surface of monocytes with GQDs was achieved by a derived peptide with a CD47 IgV domain ((Pal)-Gk (Rhodamine B) LeivtkGersletvectynG, ChinaPeptide Co., Ltd., Shanghai, China), abbreviated as CD47p here. The conjugation between the amino-functionalized GQDs (GQDs-NH<sub>2</sub>, Nanjing XFNANO Materials Tech Co.,Ltd.) and CD47p was achieved by coupling with 1-(3-(dimethylamino)propyl)-3-ethylcarbodiimide and N-hydroxysuccinimide (EDC/NHS, aladdin). Briefly, 20 mg of EDC and 10 mg of NHS were sequentially added to a solution (1 mg mL $^{-1}$ , pH = 6.0) of CD47p, and the mixture was shaken for 30 min. A solution of GQDs-NH<sub>2</sub> (1 mL) was added to the mixture, and the reaction was gently stirred for 24 h at room temperature. To remove residual EDC and NHS, the solution was dialyzed (MWCO, 1000) for 48 h (the dialysate was replaced every 12 h). The product of the conjugation of GQDs-NH<sub>2</sub> and CD47p is abbreviated here as solution B (pH = 7.44). Then, 2.5 mg of sulfosuccinimidyl 6-(3'-[2-pyridyldithio]-propionamido) hexanoate (sulfo-LC-SPDP, Sigma) was added to solution B, and the mixture was allowed to react at room temperature for 1 h. Then, the conjugate was centrifuged twice through centrifugal filtration with a molecular weight cutoff of 100 kDa (Millipore) for 5 min to remove excess sulfo-LC-SPDP cross-linkers. Then, 20  $\mu$ L of miR223 was added to the cells in the dark, and the mixture was stored in a 4 °C refrigerator overnight. A surface-engineered gene system of CD47p-GQDs-miR223 was successfully prepared.

Sequentially, the prepared CD47p-GQDs-miR223 were coincubated with monocytes (DiO-labeled) for 12 h to generate the engineered cell therapy system. A 90 Plus PALS laser particle sizer (Brookhaven, USA) was used for recording the CD47p-GQD particle size, and FT-IR spectroscopy (Bruker, USA) was used for detecting characteristic bands. An Ultra-Micro spectrophotometer (Thermo, USA) and a fluorescence spectrophotometer F-7000 (HITACHI, Japan) were used for qualitative analysis of disulfide bonds at the conjunction of CD47p-GQDs-miR223. A laser scanning confocal microscope (LSCM, Nikon, Japan) was used to acquire image information from the engineered monocytes (E-Ms).

### 2.3. Animal surgery procedure and dosing schedule

*Apoe* $^{-/-}$  mice were anesthetized with isoflurane via inhalation through a nose mask and maintained at 37 °C using a heating pad throughout the surgery. Next, the anterior cervical triangles were accessed via a sagittal anterior neck incision. The right common carotid artery (RCCA) was isolated from the circumferential connective tissues by blunt dissection, and the exposed branches of the RCCA were permanently ligated with a surgical suture (7-0 silk) at 1 mm and 4 mm below the common carotid artery bifurcation. Additionally, a spacer was adopted for ligation to control stenosis. After confirming that blood flow was present through the RCCA, the incision was closed with sutures (6-0 silk).

After surgery, the mice were fed a high-fat diet (Research Diets D12108C, 1.25 % cholesterol) for 6 weeks, after which carotid artery plaques formed. The *Apoe* $^{-/-}$  model mice were randomly divided into four groups: the CT group (without any treatment), monocyte-treated group, combination of CD47p-GQD-miR223-treated group, and engineered monocyte (M-CD47p-GQD-miR223)-treated group. The mice were injected through the tail vein every two days, and treatments were continued for 4 weeks in total. After finishing all the treatments, the

mice were euthanized, and their serum, common carotid artery, and organ tissues were collected.

#### 2.4. Evaluation of the therapeutic efficacy of M-CD47p-GQDs-miR223 *in vivo*

Furthermore, we evaluated the expression of CD86 (M1 marker) (Invitrogen, USA) and CD206 (M2 marker) (Invitrogen, USA) to assess the macrophage polarization pattern in the AS microenvironment through laser confocal microscopy (Nikon, Japan). The growth of muscle fibers and collagen fibers was evaluated and observed using an inverted microscope (Thermo, US) after Masson staining.

#### 2.5. Statistical analysis

All the data are representative of at least three experiments with similar results performed in triplicate unless otherwise indicated. The experimental data were statistically analyzed using Origin software, and the results are expressed as the mean  $\pm$  standard deviation (mean  $\pm$  SD). Tests were used for comparisons between two sets of samples, and one-way ANOVA was used for comparisons between multiple sets of samples. Differences were regarded as significant when the P value was less than 0.05 (\* $p$  < 0.05).

More detailed methods are provided in the Supporting Information.

### 3. Results

#### 3.1. Preparation of CD47p-GQDs and exploration of CD47p-engineered cells

We first investigated the optimal concentrations of CD47p and GQDs for RAW264.7 cells to determine the potential impact of CD47p and GQDs on cell viability. The CCK-8 assay results indicated that CD47p started to reduce cell viability at concentrations of  $40 \mu\text{g mL}^{-1}$  (Fig. 1a) and  $60 \mu\text{g mL}^{-1}$  (Fig. 1b) for GQDs. Therefore, we selected  $20 \mu\text{g mL}^{-1}$  for CD47p and  $40 \mu\text{g mL}^{-1}$  for the GQDs as the optimal working concentrations for subsequent studies. The cross-linking of CD47p and GQDs was achieved through the activation of carboxyl and amino groups using EDC and NHS, as depicted in Fig. 1d. Fourier transform infrared (FT-IR) spectroscopy (Fig. 1e) demonstrated that the amino graphene quantum dots (GQDs-NH<sub>2</sub>) exhibited strong stretching vibrations of C-OH near  $3300 \text{ cm}^{-1}$ , stretching vibrations of C-N near  $1285 \text{ cm}^{-1}$ , and vibrations of the graphene skeleton near  $1569 \text{ cm}^{-1}$  [29]. The infrared spectral peak signals observed in the blue curve of CD47p-GQDs within the range of  $1000\text{--}1500 \text{ cm}^{-1}$  overlapped with the corresponding peaks of GQD-NH<sub>2</sub> (red curve), indicating the successful cross-linking of CD47p and GQD-NH<sub>2</sub>. The change in particle size also confirmed the formation of the CD47p-GQD complex. As shown in Fig. 1f, the size of the CD47p-GQDs was  $379.45 \pm 21.20 \text{ nm}$ , which is significantly greater than the individual sizes of CD47p ( $367.16 \pm 31.34 \text{ nm}$ ) or the GQDs-NH<sub>2</sub> ( $292.52 \pm 7.07 \text{ nm}$ ) (Fig. 1c and Fig. S1).

The construction of CD47p-engineered cells is achieved through the binding of CD47 to SIRP $\alpha$  [32], which is a transmembrane protein found on phagocytes. To confirm the interaction between CD47p and SIRP $\alpha$ , we incubated rhodamine B-labeled CD47p with RAW264.7 cells (DiO-labeled membrane) and observed the binding-release characteristics of this complex at multiple time points by laser confocal microscopy. Fig. 1g demonstrate the colocalization of red and green fluorescence on the surface of RAW264.7 cells after 6 h. Furthermore, no detachment was observed within 24 h, indicating the stable binding of the CD47p-SIRP $\alpha$  complex to the surface of RAW264.7 cells. At 36 h, the fluorescence of CD47p detached significantly from the cell membrane surface, while fluorescence colocalization was observed in the nucleus. We hypothesize that the binding of CD47p to SIRP $\alpha$  is a time-dependent dynamic process and that its effective binding persists for more than 24 h until CD47p is naturally shed. This discovery may establish a temporal

framework for the *in vivo* transport and release of CD47p-engineered cells loaded with genetic drugs.

#### 3.2. The architecture of the engineered monocyte therapy system

After successfully generating CD47p-engineered monocytes, we further proceeded to develop a therapeutic system for engineered monocytes loaded with the gene drug ‘backpack’. The process of preparing the gene drug ‘backpack’ CD47p-GQDs-miR223 is depicted in Fig. 2a. As shown in Fig. 2a, we initially functionalized CD47p with GQDs-NH<sub>2</sub> by cross-linking carboxyl and amine groups. Subsequently, a sulfide-containing linkage was introduced to the prepared CD47p-GQDs via the use of Sulfo-SPDP-LC to facilitate miR223 loading [29]. To confirm the successful loading of miR223, we performed extracellular cleavage of the disulfide linkage by dithiothreitol (DTT). As shown in Fig. 2b, the fluorescence of the DTT-treated CD47p-GQD-S-/-S-miR223 solution significantly decreased (blue curve) compared to that of the CD47p-GQD-S-miR223 solution without DTT exposure (red curve). Additionally, we quantitatively analyzed the amount of free miRNA after complete cleavage by DTT to determine the miRNA concentration in combination with the CD47p-GQDs. As shown in Fig. 2c, the approximate content of miR223 loaded in the CD47p-GQDs-S-S-miR223 system was estimated to be  $10.83 \text{ ng } \mu\text{L}^{-1}$ . These results confirmed the successful synthesis of CD47p-GQDs-miR223 and the determination of the gene regulator content for the subsequent cell therapy system.

Immediately after preparing CD47p-GQDs-miR223 (rhodamine B-labeled), the cells were cocultured with monocytes to create an engineered cell therapy system. Laser confocal 3D images (Fig. 2d) revealed that CD47p-GQDs-miR223 remained concentrated around monocytes for more than 24 h, indicating that it could stabilize on the monocyte surface similarly to CD47p. At 36 h, CD47p-GQDs-miR223 began to shed from monocytes due to termination of the CD47p-SIRP $\alpha$  interaction, consistent with the findings from the CD47p-engineered cells shown in Fig. 1g. Furthermore, we observed that a portion of the self-shedding CD47p-GQDs-miR223 was taken up by other engineered cells instead of rebinding to the membrane through CD47p-SIRP $\alpha$ , indicating that the interaction between CD47 and SIRP $\alpha$  is time sensitive and irreversible.

#### 3.3. Innate trafficking behavior of the surface-engineered monocyte therapy system

It is unclear whether CD47p-GQD-miR223-engineered monocytes can maintain a natural trafficking behavior similar to that of endogenous monocytes in the recruitment of AS plaques; thus, we conducted this study using *in vitro* Transwell chamber assays. Fig. 3a and b shows that the number of migrated cells per field was significantly greater in the MCP-1 ( $200 \mu\text{g L}^{-1}$ ) treatment group than in the control group. These findings indicate that MCP-1 can promote the migration of both monocytes and engineered monocytes. Moreover, even at high concentrations ( $400 \mu\text{g L}^{-1}$ ), MCP-1 enhanced the migration of engineered monocytes (additional details are presented in Fig. S2).

#### 3.4. Activation of the ‘Don’t eat me’ signal relies on the CD47p-SIRP $\alpha$ complex

Like monocytes, myeloid cells express SIRP $\alpha$ , a transmembrane signal regulatory protein. When it binds to CD47, it can transmit the command ‘Don’t eat me’ and inhibit macrophage phagocytosis. To verify the interaction between CD47p-GQDs-miR223 and SIRP $\alpha$ , an anti-mouse CD172 $\alpha$  (SIRP $\alpha$ ) antibody labeled with FITC was utilized for immune recognition of the SIRP $\alpha$  protein on the monocytes’ surface. As shown in Fig. 3c, when CD172 $\alpha$  antibody was introduced to both the solitary RAW264.7 cells (M) group and the CD47p-GQDs-miR223 engineered monocyte (M + CD47p-GQDs-miR223) group, flow cytometry analysis indicated a significant reduction in the relative

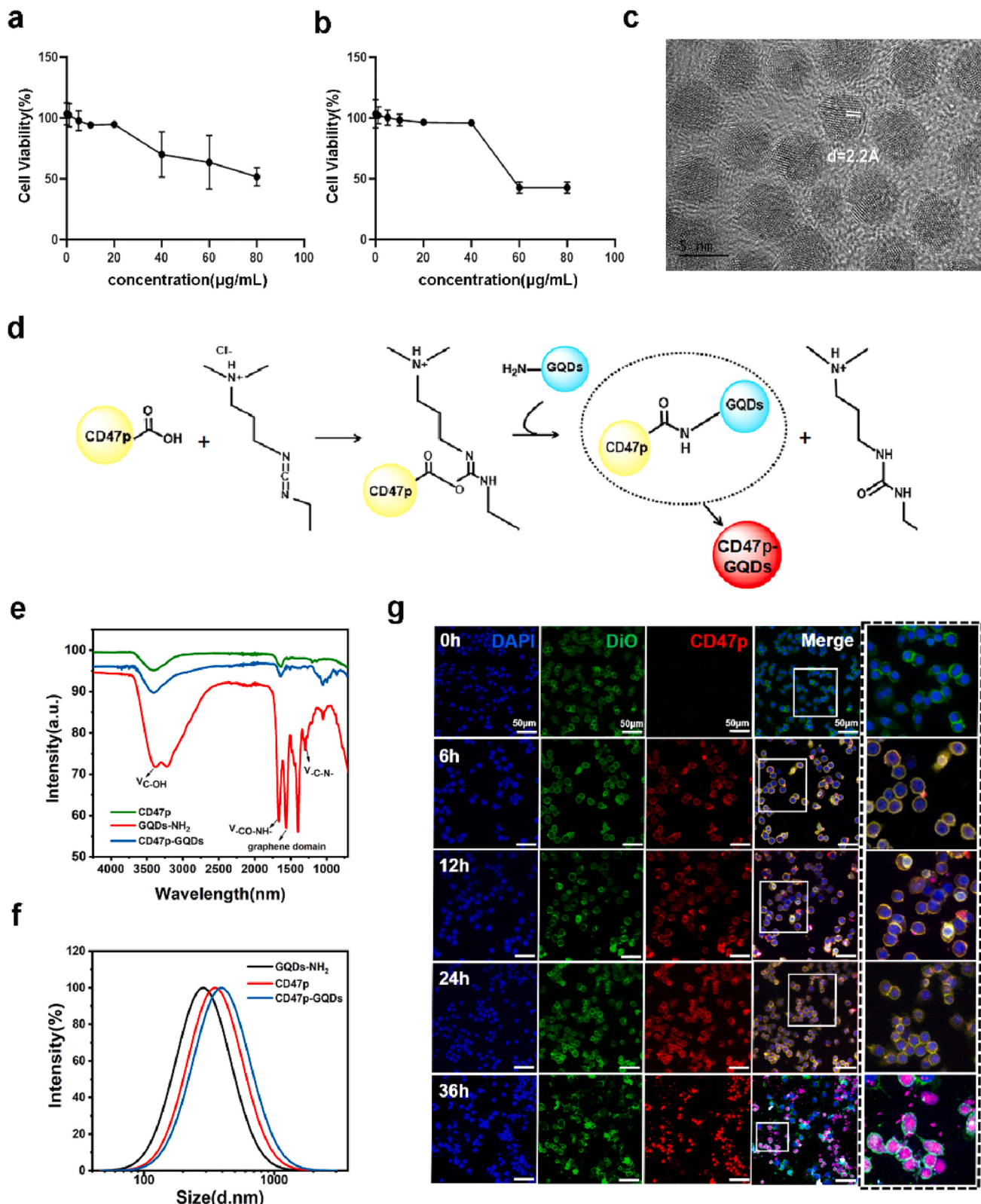


**Fig. 1.** Preparation and characterization of CD47p-GQDs and preliminary exploration of CD47p-engineered cells. Evaluation of the effect of a) CD47p and b) GQDs-NH<sub>2</sub> at different concentrations on the viability of RAW246.7 cells. c) HRTEM image of the GQDs-NH<sub>2</sub>. d) Schematic diagram of the crosslinking process between CD47p and GQDs. e) FT-IR spectra of CD47p, GQD-NH<sub>2</sub> and CD47p-GQDs. f) Particle size distribution of CD47p, GQD-NH<sub>2</sub> and CD47p-GQDs using dynamic light scattering (DLS). Note: This measurement encompasses water molecules, specifically referring to the hydrodynamic diameter. g) Confocal fluorescence images of CD47p-engineered monocytes at different times from 0 to 36 h (40X). Red fluorescence indicates rhodamine B bound to the peptide, green fluorescence indicates cell membrane-labeled DiO, and blue fluorescence indicates DAPI. Images are representative of  $n = 3$  independent experiments. The data in the figures represent the means  $\pm$  SDs.

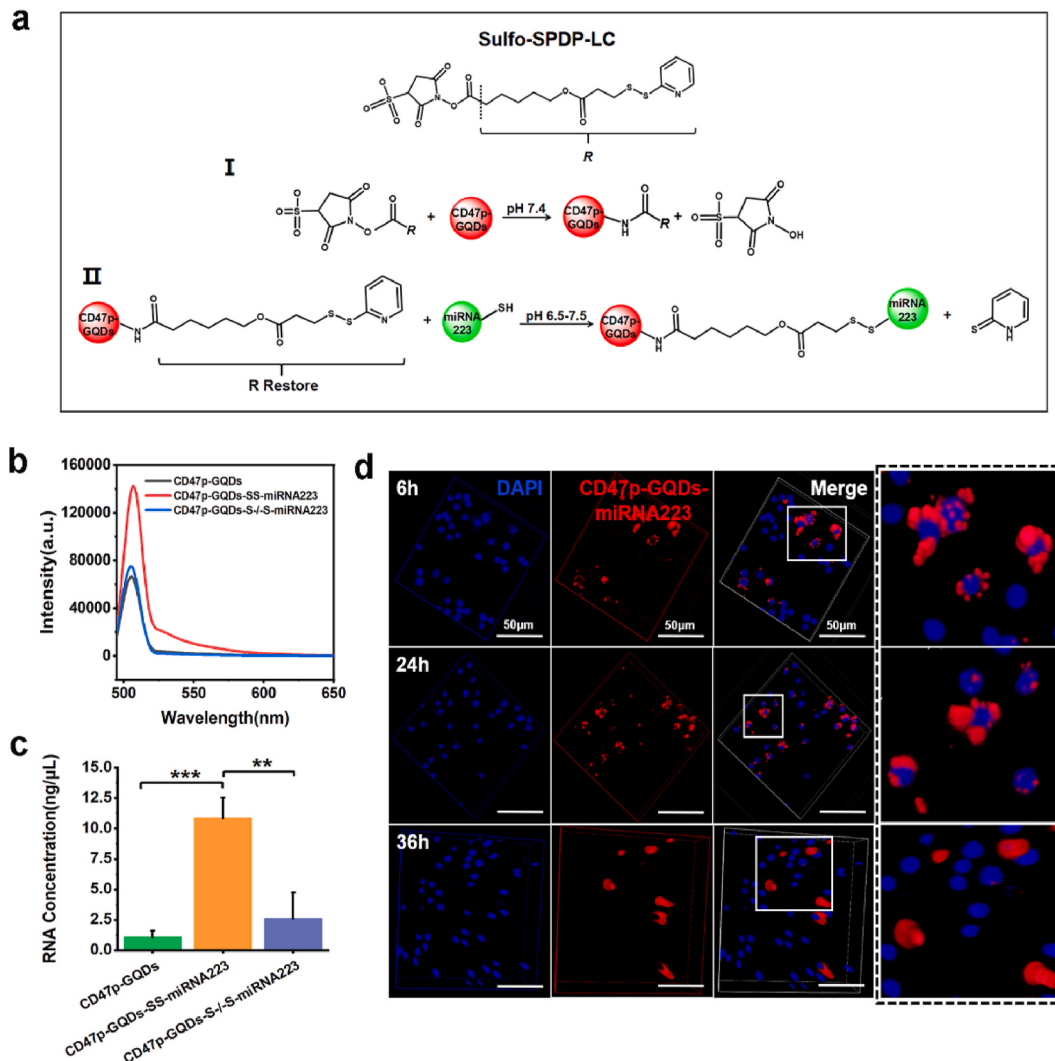


**Fig. 2.** Construction and characterization of the engineered cell therapy system. a) Schematic diagram of the crosslinking process between CD47p-GQDs and miR223. b) Fluorescence spectra of CD47p-GQDs (black) and FAM-labeled CD47p-GQDs-miR223 before (red) and after DTT treatment and filtration (blue). c) Comparisons of miR223 levels in CD47p-GQDs-miR223 before and after DTT treatment. d) 3D confocal fluorescence images of CD47p-GQD-miR223-engineered monocytes at different times from 0 to 36 h. Red fluorescence indicates rhodamine B bound to the peptide, and blue fluorescence indicates DAPI. Images are representative of  $n = 3$  independent experiments. The data in the figures represent the means  $\pm$  SDs. Significant differences: \*\* $p < 0.01$ , \*\*\* $p < 0.001$ .

fluorescence intensity (green column) of FITC in the M + CD47p-GQDs-miR223 group compared to the M group (pink column). This implies the attachment of CD47p-GQDs-miR223 to the SIRP $\alpha$  protein on the monocytes' surface through the SIRP $\alpha$ -CD47 interaction.

Immediately, polystyrene (PS) microparticles mimicked apoptotic cells and other debris *in vitro* to confirm whether macrophages retain their clearance capability following activation of the CD47p-SIRP $\alpha$  signaling pathway. A SIRP $\alpha$  polyclonal antibody was utilized as a substitute for CD47p to bind to SIRP $\alpha$  and determine if the specific activation of phagocytosis inhibition in macrophages depends solely on the CD47p-SIRP $\alpha$  interaction. As shown in Fig. 3c and Fig. S3, although both CD47p-GQDs-miR223 and the SIRP $\alpha$  polyclonal antibody had similar binding abilities to SIRP $\alpha$  on monocytes, their effects on phagocytosis were opposite. As expected, both CD47p- and CD47p-GQD-miR223-engineered monocytes significantly inhibited the phagocytosis of PS microparticles, while monocytes treated with the SIRP $\alpha$  polyclonal antibody retained their original phagocytosis ability (Fig. 3d and e). This suggests that the CD47p-SIRP $\alpha$  interaction may negatively impact the normal clearance of macrophages *in vivo*.

In atherosclerosis, the equilibrium of macrophage-controlled cholesterol handling is disrupted. The augmented buildup of ox-LDL in

cells, along with the obstruction of cholesterol efflux from the cells, speeds up the pathological process by contributing to the inflammatory immune response to create foam cells [33]. Consequently, decreasing scavenger receptor-mediated lipid uptake by macrophages is viewed as a key approach for decreasing foam cell formation [34]. Following this strategy, we developed CD47p-GQD-miR223-engineered monocytes. Consistent with the phagocytosis of PS microparticles shown in Fig. 3d and e, monocytes modified with CD47p (M-CD47p group) and CD47p-GQDs-miR223 (M-CD47p-GQDs-miR223 group) exhibited significantly suppressed uptake of ox-LDL due to the interaction of CD47p-SIRP $\alpha$ . As a result, the accumulation of intracellular lipid droplets significantly decreased, as depicted in Fig. 3f and g. Herein, we believe that as a substitute for endogenous monocytes, CD47p-GQD-miR223-engineered monocytes can inhibit the uptake of ox-LDL and reduce the accumulation of intracellular lipoproteins after they differentiate into engineered macrophages in the intima.

### 3.5. Effect of CD47p-GQDs-miR223 on the inflammatory response *In vitro*

MiR223 plays a crucial role in the immune system and can regulate

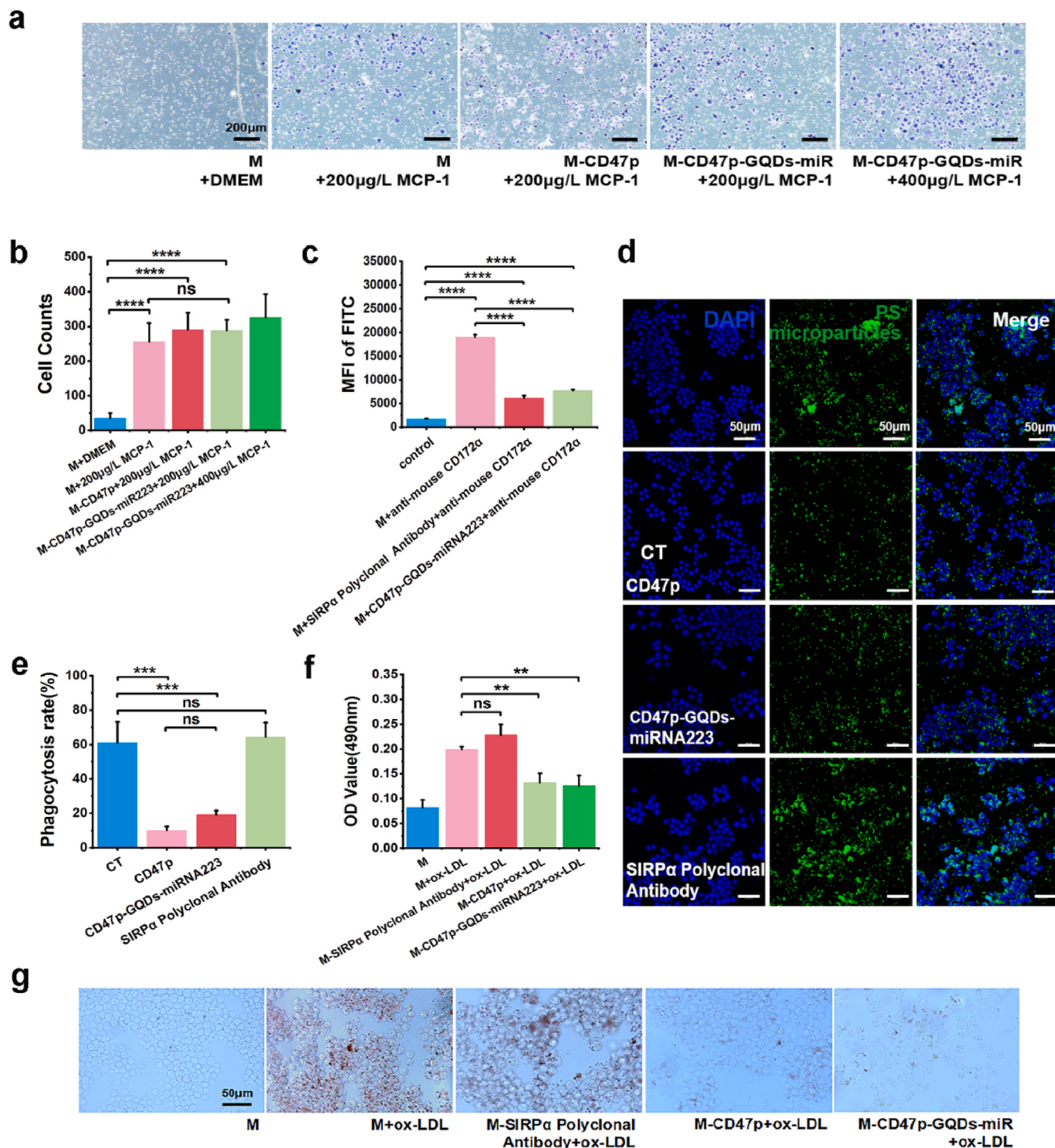


**Fig. 3.** Phagocytosis of monocytes activated by the CD47-SIRP $\alpha$  signaling pathway. a) Images of the Transwell migration of cells in each group: M + DMEM, M + 200  $\mu$ g L $^{-1}$  MCP-1, M-CD47p + 200  $\mu$ g L $^{-1}$  MCP-1, M-CD47p-GQDs-miR223 + 200  $\mu$ g L $^{-1}$  MCP-1 and M-CD47p-GQDs-miR223 + 400  $\mu$ g L $^{-1}$  MCP-1. M indicates monocyte. Transwell chamber assays showing that MCP-1 (200  $\mu$ g L $^{-1}$ ) increases the migration of both normal monocytes and surface-engineered monocytes. b) Cell counts of Transwell migration in each group. c) Flow cytometry quantification of the average fluorescence intensity of the FITC-CD172 $\alpha$  protein in different groups: blank, M, M + SIRP $\alpha$  polyclonal antibody, and M + CD47p-GQDs-miR223. FITC-conjugated anti-CD172 $\alpha$  monoclonal antibody was used to react with SIRP $\alpha$ . d) Laser confocal images of PS microparticles taken up by CT-, CD47p-, CD47p-GQD-miR223- and SIRP $\alpha$ -conjugated polyclonal antibody-treated cells. Green fluorescence indicates PS microparticles, and blue fluorescence indicates DAPI. e) Statistical analysis of PS microparticle uptake in each group. f) Quantification of the extracted intracellular Oil Red O. g) Microscopy images of ox-LDL taken up by the blank, M, M-SIRP $\alpha$  polyclonal antibody, M-CD47p and M-CD47p-GQDs-miR223 groups. An *in vitro* foam cell model was constructed by adding 40  $\mu$ g mL $^{-1}$  ox-LDL to monocytes, and we verified the results by Oil Red O staining (for specific staining of intracellular lipid droplets). Images are representative of n  $\geq$  3 independent experiments, unless otherwise noted. The data in the figures represent the means  $\pm$  SDs. Significant differences: \*p < 0.05, \*\*p < 0.01, \*\*\*p < 0.001, and \*\*\*\*p < 0.0001.

the expression of various inflammation-related genes in monocytes and macrophages [35]. Our previous research demonstrated that miR223 effectively controls macrophage polarization by stimulating alternative anti-inflammatory pathways and suppressing classic proinflammatory pathways [29]. However, it remains unclear whether CD47p-GQDs-miR223 can exert its intended inflammatory regulatory effect on macrophages. Therefore, we investigated the impact of CD47p-GQDs-miR223 in this context. Proinflammatory M1 macrophages were prioritized for LPS induction (Figure S4 a), and the expression of the classic phenotypic marker CD86 in M1-type RAW264.7 cells was quantified via flow cytometric analysis. Fig. S4b illustrates that a minimum of 78.3 % of M1 RAW264.7 cells were generated.

GQDs-miR223 were initially coincubated with the aforementioned

M1 RAW264.7 cells for 6 h (Figure S5 a). Subsequently, we assessed the serum levels of macrophage-produced cytokines, which included C-reactive protein (CRP), TNF- $\alpha$ , IL-10, TGF- $\beta$ 1 and matrix metalloproteinase-9 (MMP-9), over a 72-h period. As depicted in Fig. 4a-e, the level of the proinflammatory cytokine TNF- $\alpha$  decreased sharply as a function of time, whereas the levels of the anti-inflammatory cytokines IL-10 and TGF- $\beta$ 1 significantly increased. Similarly, the expression of both CRP and MMP-9 was attenuated, following a trend similar to that of the proinflammatory cytokine TNF- $\alpha$ . To validate the change in the M1/M2 phenotype, we monitored the *in situ* alteration of the macrophage phenotype using immunofluorescence staining and flow cytometry, as illustrated in Figs. S5b and c. As anticipated, the M1 protein marker CD86 was inhibited, whereas the M2 protein marker CD206 was strongly activated. These findings indicate

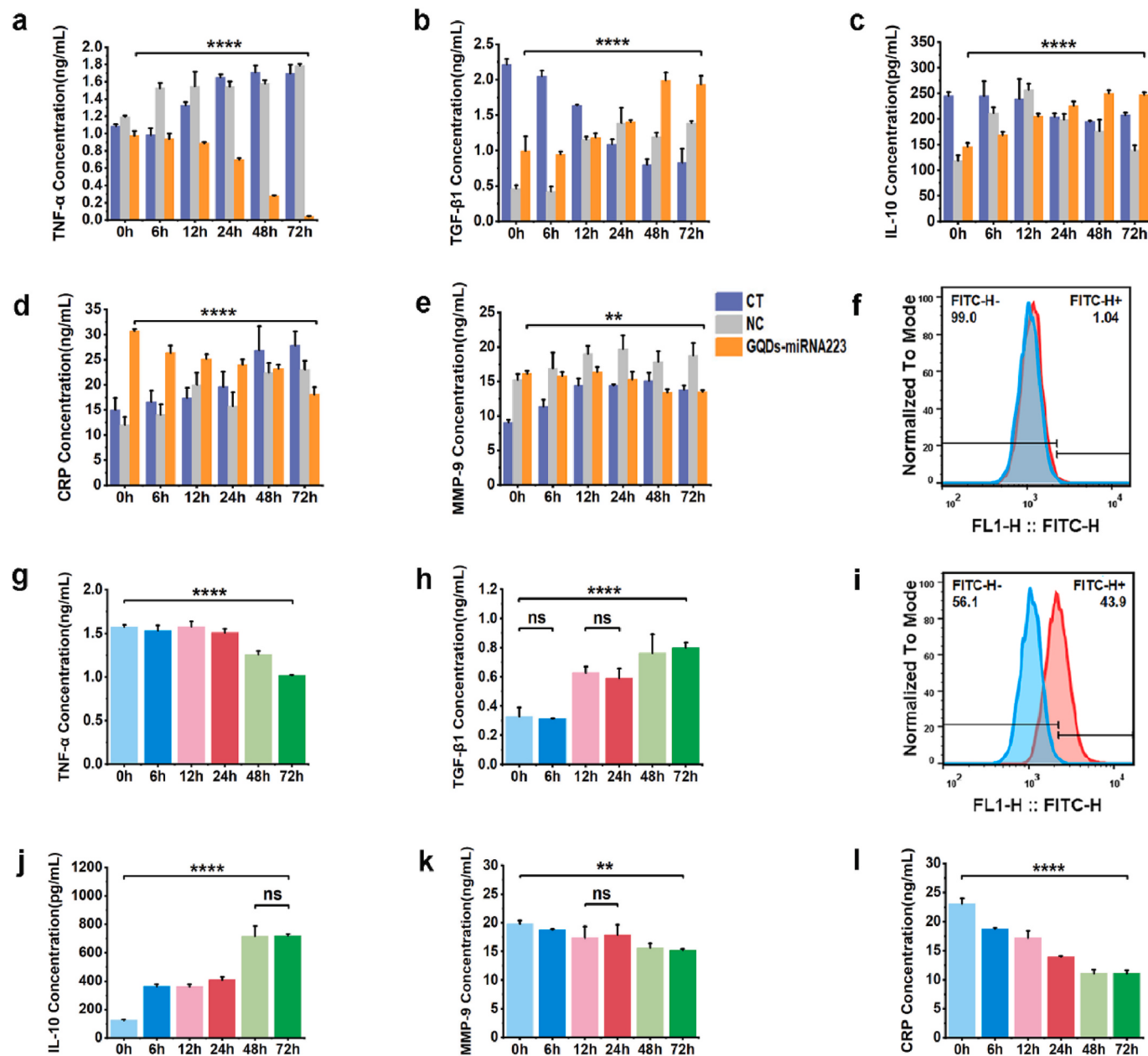


**Fig. 4.** Related molecular biological evaluations of miR223 regulation *in vitro*. ELISA was used to detect the secretion of cytokines in GQD-miR223-regulated macrophages: a) TNF- $\alpha$ , b) TGF- $\beta$ 1, c) IL-10, d) CRP and e) MMP-9. The percentage of RAW264.7 cells transfected with miR223: f) CD47p-GQDs-miR223 and i) SIRP $\alpha$  polyclonal antibody + CD47p-GQDs-miR223. ELISA detection of macrophage cytokine production regulated by CD47p-GQDs-miR223: g) TNF- $\alpha$ , h) TGF- $\beta$ 1, j) IL-10, k) MMP-9 and l) CRP. Images are representative of  $n = 3$  independent experiments. The data in the figures represent the means  $\pm$  SDs. Significant differences: \*\* $p < 0.01$ , \*\*\*\* $p < 0.0001$ .

that intracellular miR223 plays a significant role in regulating cell phenotype and inflammation.

In contrast to direct transfection and regulation of GQD-miR223 in macrophages, the uptake of CD47p-GQDs-miR223 by macrophages occurred only after termination of CD47p-SIRP $\alpha$ . To facilitate the rapid endocytosis of CD47p-GQDs-miR223 into macrophages, a polyclonal SIRP $\alpha$  antibody was used to block the binding of CD47p-SIRP $\alpha$ . The specific experimental procedures at different time points are outlined in Fig. 5a. Flow cytometry analysis revealed that CD47p-GQD-miR223 transfection in macrophages was inhibited by CD47p-SIRP $\alpha$  binding (Fig. 4f), whereas the SIRP $\alpha$  polyclonal antibody-occupied group exhibited significant phagocytosis of CD47p-GQD-miR223, with a transfection rate of approximately 43.9 % (Fig. 4i).

Although the transfection efficiency of intracellular CD47p-GQDs-miR223 on macrophages is lower than that of GQD-miR223, which achieves 68 % transfection efficiency [29], this approach can still effectively carry out its regulatory functions. Fig. 4g, h, j, k and l demonstrate a significant reduction in the expression of TNF- $\alpha$ , MMP-9 and CRP within 72 h, respectively, along with a noticeable increase in the expression of IL-10 and TGF- $\beta$ 1. Additionally, similar to GQD-miR223, CD47p-GQD-miR223 effectively regulated the macrophage phenotype (Fig. S6). Based on the above findings, we believe that CD47p-GQD-miR223 detached from monocytes, once taken up by macrophages in the plaque, whether they are resident macrophages or all monocyte-derived macrophages, initiates regulation of macrophages.

### 3.6. Concurrent 'phagocytosis inhibition' and 'inflammation regulation' orchestrated by engineered monocytes

We established an *in vitro* AS-related foam cell model to study if engineered monocytes can both regulate lipid metabolism by blocking ox-LDL uptake by macrophages and decrease plaque inflammation within the CD47-SIRP $\alpha$  binding timeframe, as illustrated in Fig. 5a and b. After CD47p-GQD-miR223-engineered monocytes (represented by the blue color in Fig. 5b) transmigrated into the arterial intima, they differentiated into engineered M1 phenotype macrophages (represented by the green color). Within 24 h, the engineered M1 macrophages were unable to phagocytose ox-LDL before the shedding of CD47p-GQD-miR223. It is likely that M1 macrophages specifically respond to ox-LDL [36], and surface modification of different macrophage types with CD47 preferentially reduces M1 macrophage phagocytosis [37]. The phagocytosis inhibition observed now aligns with the 24-h optical density (OD) value of ox-LDL uptake in Fig. 5d, indicating a notable decrease in ox-LDL uptake by macrophages. Within 36 h, the CD47p-SIRP $\alpha$  binding gradually ended. Subsequently, CD47p-GQDs-miR223 automatically detached and was absorbed by surrounding macrophages, along with certain autologous carrier cells. This led to a resumption of phagocytosis because the CD47p-SIRP $\alpha$  binding had ceased. As a result, the OD value at 36 h indicated a slight rise in ox-LDL uptake.

After 48 h, once the binding of CD47p-SIRP $\alpha$  was fully terminated, all macrophages in the environment resumed ox-LDL phagocytosis entirely. During this timeframe, the release of CD47p-GQDs-miR223, which is internalized by environmental macrophages, effectively controls inflammation and shifts M1 macrophages towards the M2 anti-inflammatory phenotype. This was further validated by findings demonstrating an *in situ* change in macrophage phenotype at the corresponding 24-h mark (Fig. 5c and Fig. S6). As depicted in Fig. 5c and Fig. S6, the notably increased average fluorescence intensity of CD206/CD86 at 24 h signified robust activation of the M2 protein marker CD206, with no repolarization occurring within 48 h. In contrast to M1 macrophages, M2 macrophages exhibit heightened ox-LDL cholesterol uptake [38], aligning with the elevated OD values at 48 h and 72 h illustrated in Fig. 5d. In summary, the concurrent 'phagocytosis inhibition' and 'inflammation regulation' orchestrated by engineered monocytes manifested within 36 h, as dictated by the CD47-SIRP $\alpha$  binding

duration.

### 3.7. Differential expression of lipid metabolism-and inflammation-related genes associated with AS plaque progression

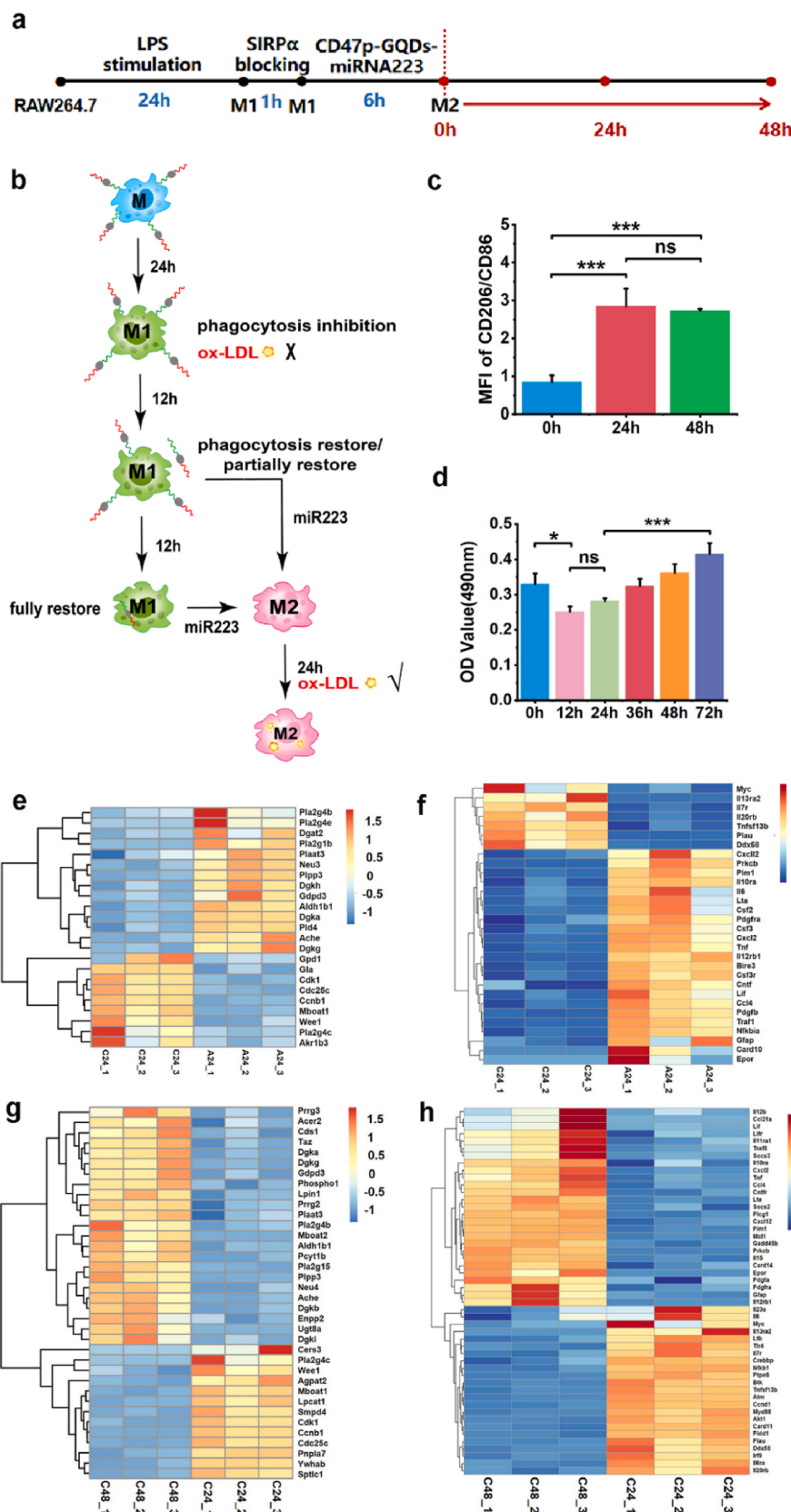
We subsequently conducted additional genome sequencing to validate the concurrent 'phagocytosis inhibition' and 'inflammation regulation' in the simulated plaque microenvironment involving engineered monocytes. Fig. 5e clearly shows that several genes related to lipid metabolism, particularly those associated with the progression of AS plaques, underwent changes. For instance, Plpp3, which was previously overlooked as a component of the risk mechanism for coronary artery disease, exhibited upregulated expression in the A24 group, suggesting ongoing lipid metabolism in M1 macrophages within 24 h. Additionally, in cases of inflammation and injury, Plpp3 expression significantly increases [39]. Notably, the upregulation of NF $\kappa$ B- $\text{I}\alpha$  [40], IL12- $\text{r}\beta$ 1 [41], CCL4 [42], and IL-6 [43] shown in Fig. 5f confirmed the presence of a proinflammatory environment within 24 h. In contrast, the engineered cells with activated phagocytosis inhibition downregulated Plpp3 expression within 24 h, suggesting the sustained effectiveness of the engineered monocyte phagocytosis inhibition of ox-LDL, which is consistent with the findings shown in Fig. 5d.

As shown in Fig. 5h, the C48 group exhibited downregulated expression of IL-6/IL-6 $\alpha$ , IL-20 $\beta$  and NF $\kappa$ B-1 and upregulated expression of CCL21a and IL-10 $\alpha$ . The above findings confirm that the simulated plaque formation microenvironment achieved a shift from proinflammatory to anti-inflammatory conditions. Fig. 5g shows that the expression of Plpp3, GDPD3, Pla2g4b, and DGKG was upregulated in the C48 group, indicating that the engineered macrophages regained their ability to take up and digest ox-LDL. Overall, M2 macrophages have a greater capacity to clear and metabolize lipids than M1 macrophages in an inflammatory microenvironment dominated by the M2 phenotype [38]. We consider the phagocytic behavior of the M2 phenotype to be favorable phagocytosis, and enhanced lipid metabolism is beneficial for the subsequent repair of damaged blood vessels. Additionally, the C48 group exhibited upregulated expression of Neu4 (Fig. 5g), while the A24 group exhibited upregulation of Neu3 (Fig. 5e). Neu3 is a positive regulatory factor for leukocyte recruitment [44], whereas Neu4 has a negative regulatory role in this process. Therefore, the upregulation of Neu4 may reduce leukocyte recruitment to atherosclerotic plaque lesions.

### 3.8. Biosafety evaluation of M-CD47p-GQDs-miR223

As a cell therapy system, *in vivo* safety assessment of M-CD47p-GQDs-miR223 should be completed first. The animal modeling process is depicted in Fig. 6a. Six-week-old *Apoe*<sup>-/-</sup> mice were subjected to right common carotid artery (RCCA) surgery and were fed a high-fat diet (HFD) for 6 weeks. To confirm plaque formation after RCCA surgery, carotid artery tissue was collected from *Apoe*<sup>-/-</sup> mice and subsequently frozen, embedded and stained with Oil Red O. At 12 weeks, evident lipid plaques had formed in the arterial lumen (Fig. 6b), indicating successful establishment of the AS plaque animal model. The timeline for animal modeling and intravenous administration is provided in Fig. 6c. Throughout the entire process, the body weight and growth of the mice were monitored and recorded. Fig. S7 shows satisfactory growth in each administration group, with no significant difference in average body weight among the groups.

To confirm the good biosafety of the engineered monocyte therapy system *in vivo*, the serum alanine aminotransferase (ALT), aspartate aminotransferase (AST), creatinine (Cr) and urea (urea) levels were determined in *Apoe*<sup>-/-</sup> mice using biochemical methods. Biosafety is a major concern in cell therapy involving nanomaterials. The results indicated no significant differences in the serum ALT/AST level (Fig. 6d and e) or serum Cr/urea level (Fig. 6g and h) among the groups, suggesting that compared with the control treatment, the monocyte/C47p-



(caption on next page)

**Fig. 5.** Simultaneous regulation of lipid metabolism and inflammation *in vitro*. a) Flow diagram of the effect of CD47p-GQDs-miR223 on phagocytes. b) Time node diagram of ox-LDL uptake by M-CD47p-GQDs-miRNA223 *in vitro*. c) The average fluorescence intensity of CD206/CD86 in macrophages regulated by CD47p-GQDs-miR223 at 0, 24, and 48 h. In the supplementary time node correspondence, 0 h corresponds to 24 h in the left diagram, which means that the engineered monocytes are recruited into the arterial intima and differentiate into M1 macrophages; 24 h corresponds to 24 + 12+12 h in the left diagram, which means that the shedding CD47p-GQDs-miR223 is taken up by macrophages in the mimic AS microenvironment and polarizes M1 into the M2 phenotype; Similarly, 48 h corresponds to 24 + 12+12 + 24 h. d) The OD value statistics of ox-LDL dynamic uptake and the time nodes on the vertical axis correspond one-to-one with the left diagram. Heatmaps of e) lipid metabolism-related genes and (f) inflammation-related genes in the A24 and C24 samples. A24 represents LPS-stimulated M1 macrophages coincubated with ox-LDL for 24 h, while C24 represents CD47p-GQDs-miR223-engineered M1 macrophages coincubated with ox-LDL for 24 h. g) Heatmap of lipid metabolism-related genes in C48 samples. h) Heatmap of inflammation-related genes in C48 samples. C48 represents engineered macrophages coincubated with ox-LDL for 48 h after complete detachment of CD47p-GQDs-miR223. Images are representative of  $n = 3$  independent experiments. The data in the figures represent the means  $\pm$  SDs. Significant differences: \* $p < 0.05$ , \*\*\* $p < 0.001$ .

GQD-miR223/M-C47p-GQD-miR223 treatment did not cause renal, splenic or liver toxicity. The potential toxicity of monocyte/C47p-GQDs-miR223/M-C47p-GQDs-miR223 to vital organs was further investigated using H&E staining. As shown in Fig. 6i, no histopathological abnormalities, lesions, or degenerations were observed in the kidney, liver, or spleen in any of the four groups, confirming the good biocompatibility of the M-C47p-GQD-miR223 therapy system *in vivo*.

### 3.9. *In vivo* tracking of the engineered monocytes

Based on the *in vitro* results confirmed in Fig. 3a, which demonstrated that engineered monocytes still displayed innate trafficking behavior, we subsequently monitored their recruitment into atherosclerotic plaque lesions after intravenous injection by tracking them *in vivo*. DiR (excitation at 748 nm, red fluorescence)-stained monocytes were injected into *Apoe*<sup>-/-</sup> mice (Fig. 6f), and an *in vivo* imaging system was utilized to track the cells in the animals. Fig. 6j shows that DiR-stained monocytes and M-C47p-GQDs-miR223 accumulated in the carotid artery of *Apoe*<sup>-/-</sup> mice and exhibited noticeable fluorescence at 6 and 24 h postinjection. This finding confirmed that the natural trafficking behavior of engineered monocytes *in vivo* is unaffected by cell surface modification. Interestingly, the rhodamine B-labeled C47p-GQD-miR223 combination was observed in the carotid artery and presented relatively weak fluorescence. We hypothesize that certain C47p-GQDs-miR223 might attach to endogenous monocytes *in situ* via the CD47-SIRP $\alpha$  interaction and then move towards AS plaques.

### 3.10. Engineered monocytes remolded the anti-inflammatory microenvironment *in vivo*

Inflammation is crucial in all stages of atherosclerotic lesion development, ranging from initial lesions to advanced plaques. In atherosclerosis, the disruption of macrophage-dependent cholesterol handling occurs due to the activation of various factors, including proinflammatory cytokines [45–48]. Hence, regulating the inflammatory microenvironment in atherosclerosis is of utmost importance.

To determine whether M-CD47p-GQDs-miRNA223 could remodel the anti-inflammatory microenvironment in AS plaques, we monitored the *in situ* change in macrophage phenotype using immunofluorescence staining, as shown in Fig. 7a and c. Consistent with the *in vitro* experiments shown in Fig. 5c, the M2 protein marker CD206 (Cy3, red fluorescence) was activated, while the M1 protein marker CD86 (AF488, green fluorescence) was strongly inhibited. Similarly, the corresponding mean fluorescence intensities (MFIs) of CD206 $^{+}$  (Fig. 7b) and CD86 $^{-}$  (Fig. 7d) cells indicated that the plaques were dominated by M2 anti-inflammatory macrophages after treatment with M-CD47p-GQDs-miR223. Furthermore, compared to those in the carotid lumen of HFD-fed mice, which exhibited substantial plaque blockage, the mice treated with M-CD47p-GQDs-miR223 exhibited minor plaque obstruction in the lumen (Fig. 7e). When combined with the calculated unobstructed areas shown in Fig. 7f, the M group and CD47p-GQDs-miR223 group presented unobstructed areas of 37.82 % and 40.90 %, respectively. Interestingly, compared with the untreated mice, the mice treated with M-CD47p-GQDs-miR223 had an unobstructed area of 63.06 % and a

significant reduction in plaque area.

ELISA was further performed on inflammatory factor and AS-susceptible plaque-related factor levels in the serum of each group after different treatments to determine the therapeutic effect of M-CD47p-GQDs-miR223. The results indicated that the expression level of the anti-inflammatory cytokine TGF- $\beta$ 1 in the serum of mice treated with M-CD47p-GQDs-miR223 was significantly higher than that in the other three groups (Fig. 7h). In contrast, the expression levels of the proinflammatory cytokines TNF- $\alpha$  and MCP-1 were significantly decreased (Fig. 7g and i). Additionally, the expression level of the intercellular adhesion molecule ICAM-1, which is induced by endothelial cells (ECs) and vascular smooth muscle cells (VSMCs) [49], was significantly reduced after treatment with M-CD47p-GQDs-miR223 (Fig. 7j). The decreased expression levels of MCP-1 and ICAM-1 suggested a decrease in monocyte adhesion and recruitment in early atherosclerotic lesions. Moreover, the expression level of the matrix metalloproteinase MMP-9 dramatically decreased (Fig. 7k). The balance between collagen synthesis by VSMCs and collagen degradation by MMP-9 plays a crucial role in determining the stability of the fibrous cap, which is strongly associated with plaque rupture.

Finally, after the cells were stained with a FITC-F4/80 antibody, we isolated the cells from the carotid artery plaques of the mice and sorted the macrophages using flow cytometry. As depicted in Fig. 7l and Fig. S8, the total count of F4/80 $^{+}$  macrophages in the plaques treated with M-CD47p-GQDs-miR223 was significantly lower than that in the untreated group. This decrease in plaque macrophages can be attributed to the suppression of monocyte recruitment [50] and/or progression from the plaque by induction of the M1 migration marker CCR7 in foam cells [51–54]. In this study, reversing the inflammatory microenvironment have prevented the continuous influx of monocytes, which is beneficial for reducing the number of macrophages involved in plaque formation, and further impeded the progression of atherosclerotic plaques.

### 3.11. Engineered monocytes regulated the lipid metabolism levels *in vivo*

Atherosclerosis is a chronic inflammatory disease characterized by the defective resolution of vascular inflammation in the vessel wall and accumulation of low-density lipoprotein cholesterol (LDL-C) in the arterial system [55]. Studies indicate that patients with AS may exhibit elevated total cholesterol (TC) and triglycerides (TG) levels, along with reduced high-density lipoprotein cholesterol (HDL-C) levels, in comparison to healthy individuals [56]. Therefore, it is crucial to monitor *in vivo* lipid levels to validate the lipid metabolism-regulating effects by M-CD47p-GQDs-miR223.

We evaluated TG (Fig. S9), TC (Fig. 7m), LDL-C (Fig. 7n), and HDL-C (Fig. 7o) concentrations in the serum M-CD47p-GQDs-miR223 notably decreased TC and LDL-C levels, which are linked to an increased risk of heart disease. Conversely, it raised HDL-C levels, known as the 'good' cholesterol that aids in eliminating surplus cholesterol from the blood. Overall, the engineered monocytes showed a significant lipid lowering in the *Apoe*<sup>-/-</sup> mice.

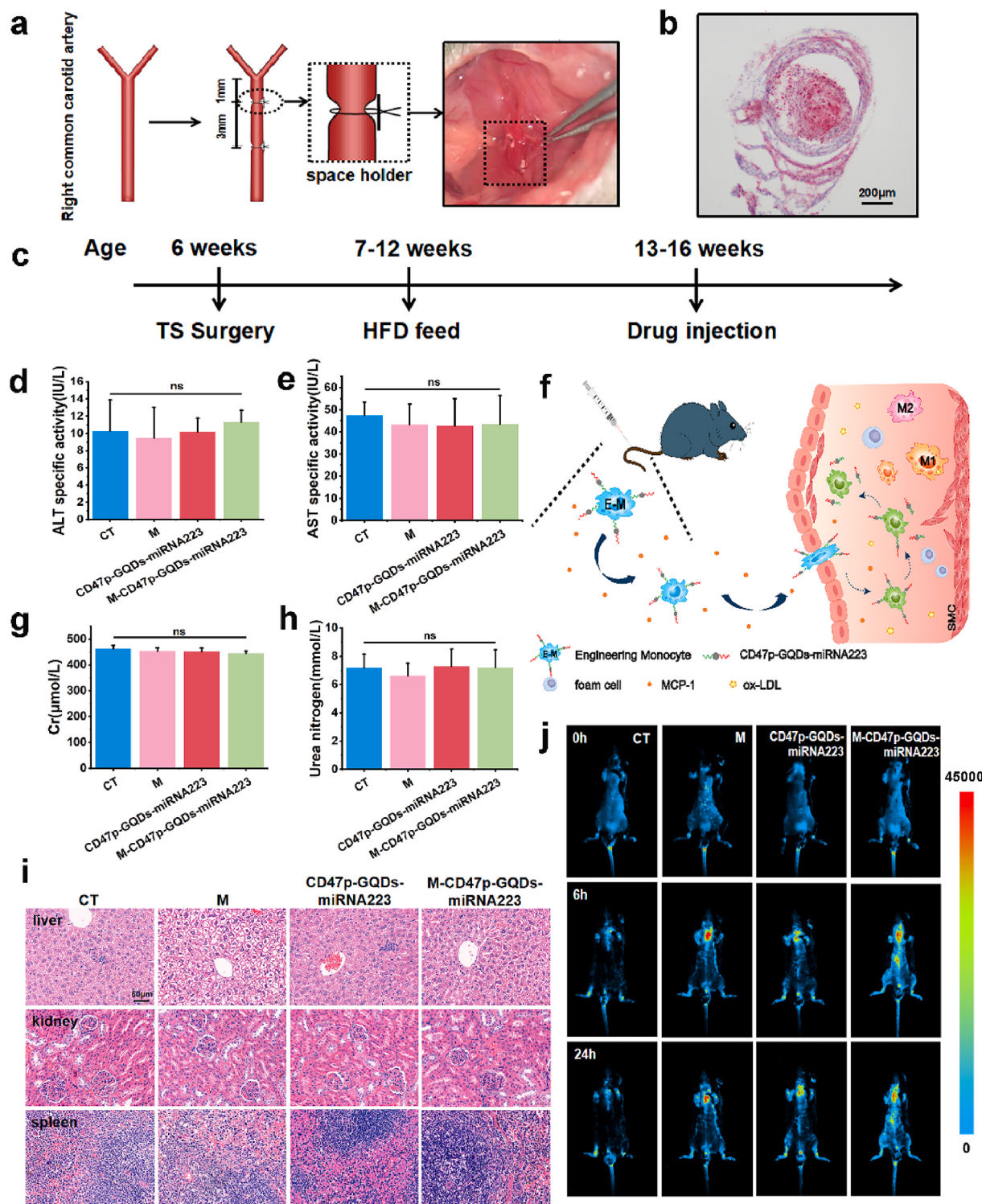


**Fig. 6.** *In vivo* treatment of engineered monocytes a) Animal modeling process: partial ligation of the RCCA in 6-week-old *Apoe*<sup>-/-</sup> mice. Right, optical photograph of the surgery. b) Oil Red O staining image of carotid artery sections; scale bar = 200 μm. c) The timeline of the animal model and intravenous administration process. The mice were fed a high-fat diet for 6 weeks after surgery, and then the mice were subjected to tail vein injection after they were fed a high-fat diet for 6 weeks. Biosafety of monocyte/CD47p-GQDs-miR223/M-CD47p-GQDs-miR223 *in vivo*. Serum levels of d) ALT, e) AST, g) Cr and h) urea at 24 h after the last treatment were measured. f) Schematic diagram of the *in vivo* transport of M-CD47p-GQDs-miR223. i) H&E staining of mouse organs (livers, kidneys and spleens) after finishing the entire treatment. j) *In vivo* imaging of mice at different time points after treatment with monocyte/CD47p-GQDs-miR223/M-CD47p-GQDs-miR223. Images are representative of n ≥ 3 independent experiments. The data in the figures represent the means ± SDs. Significant differences: ns p > 0.05.

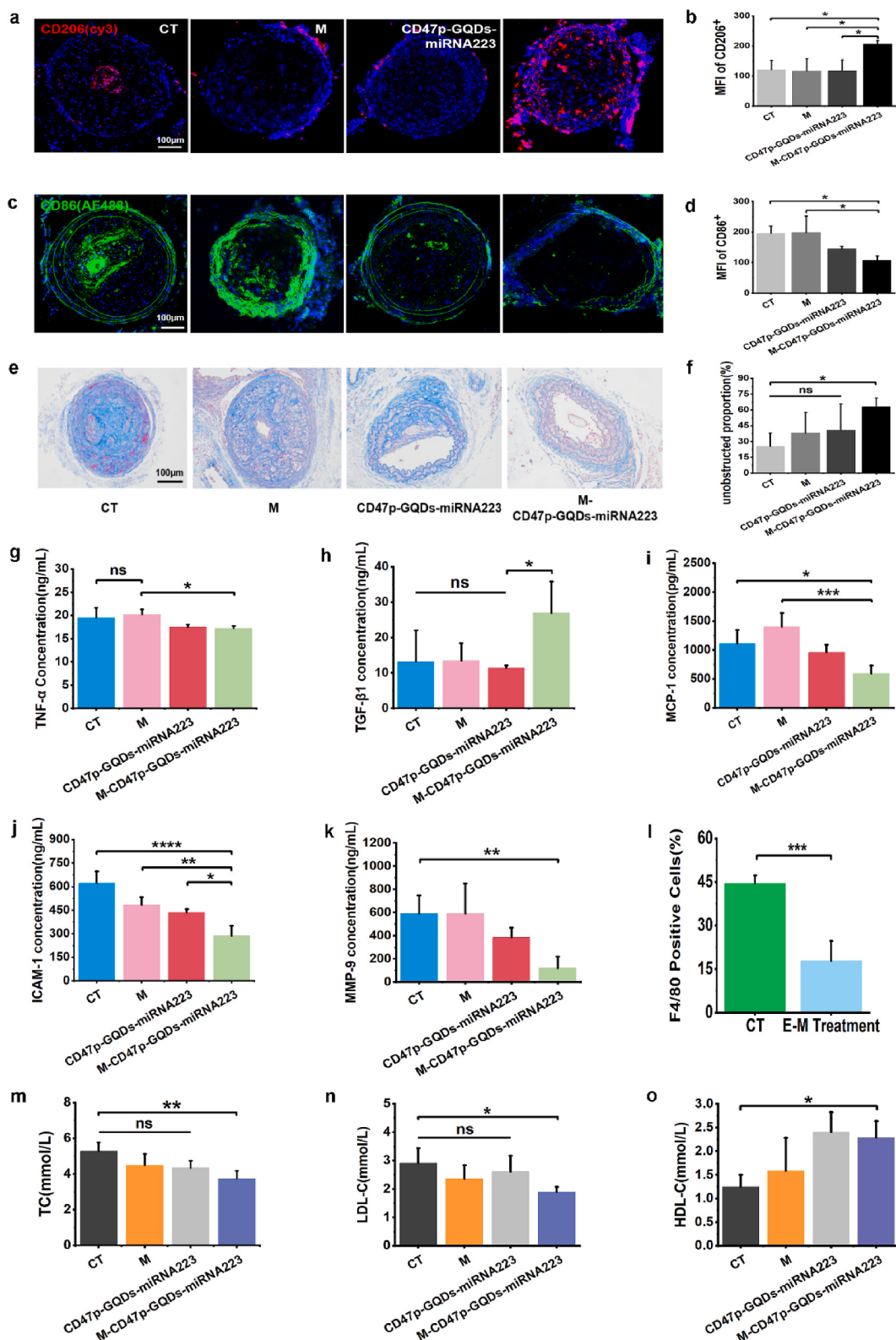


**Fig. 7.** Evaluation of the *in vivo* therapeutic effects of engineered monocytes. Immunostaining of a) CD206<sup>+</sup> (Cy3) and c) CD86<sup>+</sup> (AF488) macrophages in carotid artery tissue sections after treatment. The average fluorescence intensities of b) CD206<sup>+</sup> and d) CD86<sup>+</sup> cells in carotid artery sections. e) Masson staining image of carotid artery sections. f) Calculation of the residual cavity area of plaque slices. The *in vivo* therapeutic effect of monocyte/CD47p-GQDs-miR223/M-CD47p-GQDs-miR223 on the basis of the serum levels of g) TNF- $\alpha$ , h) TGF- $\beta$ 1, i) MCP-1, j) ICAM-1, k) MMP-9 after treatment. l) The percentage of F4/80-positive macrophages in the mouse common carotid artery was determined via flow cytometry. The *in vivo* therapeutic effect of monocyte/CD47p-GQDs-miR223/M-CD47p-GQDs-miR223 on the basis of the serum levels of m) TC, n) LDL-C and o) HDL-C after treatment. Images are representative of  $n \geq 3$  independent experiments. The data in the figures represent the means  $\pm$  SDs. Significant differences: \* $p < 0.05$ , \*\* $p < 0.01$ , \*\*\* $p < 0.001$ , and \*\*\*\* $p < 0.0001$ .

#### 4. Discussion

Atherosclerotic lesions in the early stages of atherosclerosis are characterized by the subendothelial accumulation of lipid-laden macrophages in large arteries. These lipid-laden macrophages, predominantly of the M1 type, enhance their uptake of modified LDL by expressing lipid affinity receptors including SR-A, CD36, and LOX1/SR-E1 prominently on their surface. The increased production of ox-LDL and upregulated expression of LOX-1 lead to elevated uptake of ox-LDL in M1-type macrophages, which is referred to as 'aberrant phagocytosis' or 'excessive uptake', ultimately resulting in macrophage dysfunction in lipid metabolism and the formation of foam cells. Foam cells have been shown to contribute to various atherogenic processes, including the recruitment of monocytes by producing MCP-1 [57,58], the formation of necrotic cores in atherosclerotic plaques [59], and the production of matrix metalloproteinases (MMPs).

In the past decade, several therapies for atherosclerosis have been developed, including statins, which lower cholesterol levels and may directly or indirectly impact macrophage foam cell formation [60], as well as anticytokine therapy [61] and anti-inflammatory therapy (nuclear receptor agonists [62], peroxisome proliferator-activated receptors (PPARs) [63], and liver X receptor (LXR) agonists [64,65]), which target macrophage foam cell formation and may provide clinical benefits. From a clinical perspective, intervention in the pathogenesis of atherosclerotic plaques may be an ideal strategy for regulating cytokines associated with foam cell formation or lowering serum LDL levels. However, these intervention methods may interfere with normal immune system function and may cause other side effects. Atherosclerosis is a complex disease involving multiple cellular and molecular mechanisms; therefore, there is hope that novel and safe therapies targeting foam cells can be developed for clinical use in treating atherosclerosis.

Using human and animal models, it has been clearly demonstrated that the key initial step in the formation of macrophage-derived foam cells is the migration of monocytes from the bloodstream into the subendothelial intima. Within this intima, the monocytes further differentiate into macrophages [57], which, along with vascular smooth muscle cells (VSMCs) transformed macrophages-like cells [66], contribute to the progression of atherosclerosis. Based on this, we propose a bold hypothesis: In cases of inevitable monocyte infiltration during AS development, we can use *in vitro* engineered monocytes to replace some circulating monocytes entering the intima. These monocyte substitutes can be equipped with restricted phagocytic abilities, potentially aiding in inhibiting foam cell formation. The excessive lipid phagocytosis of macrophages may be associated with altered or lost CD47 expression on apoptotic cells during early atherosclerotic plaque formation [67]. Interestingly, macrophages in advanced plaques exhibit sharply impaired phagocytosis due to the upregulated expression of CD47 molecules. Inspired by these findings, the use of monocyte substitutes with restricted phagocytic ability through the CD47-SIRP $\alpha$  signaling pathway may be an ideal strategy for reducing intracellular lipid accumulation. As shown in Fig. 3d and g, CD47p-modified monocytes exhibited significant suppression of phagocytosis of PS and ox-LDL. Considering the binding duration of CD47-SIRP $\alpha$  on monocytes shown in Fig. 1g (over 36 h) and the *in vivo* transport duration shown in Fig. 6j (just 6 h), these monocyte substitutes can efficiently inhibit the *in vivo* uptake of ox-LDL for more than 24 h.

Honestly, reducing foam cell formation simply by inhibiting the phagocytosis of ox-LDL is flawed because the removal and sequestration of modified LDL are important parts of the protective role of phagocytes in the inflammatory response [11,68]. Prolonged inhibition of phagocytosis causes lipids to accumulate in an artery, creating a vicious cycle of inflammation, lipoprotein modification, and further inflammation, which can be sustained in the artery due to the presence of these lipids. Thus, intricate approaches are required to decide when to inhibit phagocytosis and when to restore normal lipid metabolism in macrophages under specific conditions. A proinflammatory microenvironment

is the fundamental cause of excessive phagocytosis and abnormal lipid metabolism in macrophages. Evidently, inflammation attenuation and anti-inflammatory remodeling in the plaque microenvironment benefit macrophages by restoring physiological lipid metabolism. Therefore, we constructed a gene drug 'backpack' for monocytes with limited lipid phagocytosis. Following termination of CD47-SIRP $\alpha$  interactions, miR223 from the drug backpack was released. The regulation of inflammation and macrophage phenotype polarization by miR223 was confirmed, as shown in Fig. 4. M2 phenotype possesses superior phagocytic capabilities compared to M1 and can counteract the inflammation caused by M1 by modulating the release of inflammatory cytokines.

Simultaneously, we consider it crucial to restrict lipid uptake by macrophages from monocyte precursors during their shift from a proinflammatory to an anti-inflammatory state, as lipids play a significant role in macrophage polarization. For instance, ox-LDL can prompt M2 to shift towards M1 [69,70] and aid in the transformation of M2a macrophages into foam cells [71]. Thus, restricting lipid uptake to lessen the lipid burden in macrophages is advantageous for re-polarization M1 towards M2 through the influence of miR223. Once an anti-inflammatory setting is established, M2 macrophages demonstrate a strong ability to clear and repair tissues, facilitating the normalization of macrophage lipid processing and preventing foam cell development. In Fig. 5, we noted changes in genes linked to macrophage lipid processing and inflammatory agents within 72 h of CD47-SIRP $\alpha$  interaction, confirming the potential therapeutic influence of engineered monocytes on foam cell creation. Fig. 5e shows that the Pla2g4b gene was upregulated within 24 h (A24, untreated group). Pla2g4b is known to play a role in the production of various inflammatory mediators, such as prostaglandins [72], interleukins [73–75], and platelet activating factor [76]. These inflammatory mediators can contribute to the inflammatory response in the walls of blood vessels, leading to the formation and progression of atherosclerotic plaques. Engineered cells (C24, treated group) exhibited reduced Pla2g4b expression, indicating effective phagocytosis inhibition in engineered monocytes and resulting in decreased ox-LDL phagocytosis. Pla2g4b expression may be a crucial indicator of lipid metabolism instability in M1 macrophages.

Similarly, the expression of the Akr1b3 gene was downregulated within 24 h in the A24 group. Akr1b3 is associated with the breakdown of fat, and its absence can reduce obesity in individuals fed high-fat diets and increase fat breakdown [77]. The C24 group exhibited upregulated Akr1b3 expression due to the effectiveness of inhibiting ox-LDL-mediated phagocytosis. Additionally, as the uptake of ox-LDL by M1 macrophages increased, the expression of GPD3 increased, whereas that of ccb1 decreased in the A24 group. Overexpression of GPD3 can increase fatty acid uptake [78], while downregulation of the ccb1 gene may disrupt lipid metabolism by affecting the expression of key genes involved, including peroxisome proliferator-activated receptor gamma (PPAR $\gamma$ ) [79,80] and sterol regulatory element-binding protein 1c (SREBP-1c)[81], in lipid synthesis and breakdown, as well as by altering the cellular energy balance. Therefore, we speculate that the excessive phagocytosis of M1 macrophages in the proinflammatory microenvironment is related to the upregulation of GPD3 and downregulation of ccb1. Based on the above analysis, we confirmed that the inflammatory environment promotes excessive phagocytosis of ox-LDL by M1 macrophages, leading to gradual progression to foam cells without any intervention.

Fig. 5b shows that the binding of CD47p to SIRP $\alpha$  gradually terminated after 24 h. Controlled by the asynchronous termination of CD47p-SIRP $\alpha$  binding to the monocyte surface, a subset of monocyte-derived macrophages regained the ability to take up CD47P-GQDs-miR223, while the other subset continued to effectively inhibit the phagocytosis of ox-LDL. Phagocytosis inhibition and inflammation regulation occurred simultaneously until full detachment of CD47P-GQDs-miR223 from the monocyte surface, consistent with the results shown in Fig. 5c and d. Furthermore, the increased expression of IL-13r $\alpha$ 2 in C24 cells

shown in Fig. 5f is a significant signal for the activation of M2 macrophages [82]. Additionally, as shown in Fig. 5h, the expression of IL-6/IL-6 $\alpha$ , IL-20 $\beta$  and NF $\kappa$ B-1 was downregulated, while the expression of CCL21a and IL-10 $\alpha$  was upregulated in the C48 group. NF $\kappa$ B-1 plays a role in promoting the activation, aggregation, and production of inflammatory mediators in inflammatory cells, thereby exacerbating plaque inflammation [83,84]. IL-20 is expressed in atherosclerotic plaques and accelerates murine atherosclerosis *in vivo*. [85] As a receptor subunit of IL-20, IL-20 $\beta$  can bind to IL-20 and form a complex, mediating its signal transduction. CCL21a can attract endothelial cells and endothelial precursor cells, guiding them to migrate to the angiogenesis area by binding with its receptor CCR7, thereby participating in the formation of new blood vessels and tissue repair [86,87]. Furthermore, IL-10 $\alpha$  can bind to IL-10 to regulate its signal transmission, maintaining immune balance in the plaque microenvironment and preventing an excessive immune response. The increase in the IL-10 $\alpha$  level was consistent with the increase in the IL-10 level observed in Fig. 4j.

As expected, we found that intravenously injected engineered monocytes may compete with endogenous monocytes during recruitment and contribute to immune responses. The notable reduction in the total macrophage count in the arteries after the introduction of engineered monocytes (Fig. 7l) could be attributed to competitive recruitment. The upregulated Neu4 expression in Fig. 5g and the notable MCP-1 decrease (Fig. 7i) also suggest that engineered monocytes may lessen leukocyte recruitment to atherosclerotic plaque lesions. Furthermore, CD47p-GQD-miR223-engineered monocytes showed significant systemic lipid-lowering impacts (Fig. 7m–o and Fig. S9). The combination of anti-inflammatory and lipid-lowering treatments will enhance therapeutic results in atherosclerosis patients compared to individual lipid-lowering, anti-inflammatory, or anti-cytokine therapies.

## 5. Conclusion

As an advanced treatment concept for atherosclerotic plaques in its infancy, a strategy to enhance therapeutic cell therapy using engineering means to integrate nanomaterials and genetic molecules is emerging. In contrast to traditional anti-inflammatory therapies that focus on foam cells, like delivering statins, anti-foam cytokines, and nuclear receptor agonists passively into plaques to counter foam cell formation, the engineered monocyte therapy system offers the advantage of natural trafficking towards atherosclerotic lesions. More specifically, the role of monocytes in entering lesions has been completely reversed. These cells no longer primarily contribute to foam cell formation but instead aid in inhibiting it and promoting healing. By leveraging the CD47-SIRP $\alpha$  interaction for activation and termination, we successfully reversed the inflammatory environment of the lesion, decreased monocyte infiltration, and improved lipid metabolism in the early stages of treating atherosclerotic plaques. Furthermore, drawing inspiration from chimeric antigen receptor T-cell immunotherapy, our cell engineering technology presents opportunities to modify endogenous immune cells and reintroduce them, potentially for future clinical applications using monocytes obtained from human patients.

## Funding

This work was supported by Key Projects of the National Natural Science Foundation of China (81830055, 82230073); the Outstanding Scientist Project of Chongqing (cstc2022yjh-bzxm0186); and the Chongqing Key Laboratory of Prevention and Treatment for Occupational Diseases and Poisoning (2022-2023ZYBKF01).

## Data and materials availability

All the data are available in the main text or the supplementary materials.

## CRediT authorship contribution statement

**Qing Xia:** Writing – original draft, Methodology, Investigation, Formal analysis. **Feila Liu:** Writing – review & editing, Writing – original draft, Resources, Project administration, Methodology, Investigation, Conceptualization. **Yue Zhou:** Methodology. **Guanyuan Yang:** Methodology, Formal analysis. **Fangzhou Li:** Writing – review & editing, Supervision, Conceptualization. **Tingting Liang:** Methodology. **Jun Liu:** Methodology. **Wanling Li:** Methodology. **Yaqing Huang:** Methodology. **Chuhong Zhu:** Writing – review & editing, Resources, Funding acquisition, Conceptualization.

## Declaration of competing interest

The authors declare the following financial interests/personal relationships which may be considered as potential competing interests: Chuhong Zhu reports equipment, drugs, or supplies was provided by National Natural Science Foundation of China. If there are other authors, they declare that they have no known competing financial interests or personal relationships that could have appeared to influence the work reported in this paper.

## Data availability

Data will be made available on request.

## Acknowledgments

We would like to express our gratitude to Prof. Fan (Yonghong Fan, the General Hospital of the Western Theater Command of the People's Liberation Army of China) for his valuable input and assistance in refining our manuscript. His expertise and insights have greatly contributed to the improvement of our work. We sincerely appreciate Prof. Cao (Changyan Cao, Institute of Chemistry, Chinese Academy of Sciences), who helped us polish our manuscript. Thank you for your support and guidance.

## Appendix A. Supplementary data

Supplementary data to this article can be found online at <https://doi.org/10.1016/j.mtbiol.2024.101178>.

## References

- [1] Y. Gui, H. Zheng, R.Y. Cao, Foam cells in atherosclerosis: novel insights into its origins, consequences, and molecular mechanisms, *Frontiers in Cardiovascular Medicine* 9 (2022) 845942, <https://doi.org/10.3389/fcvm.2022.845942>.
- [2] W. Erl, P.C. Weber, C. Weber, Monocytic cell adhesion to endothelial cells stimulated by oxidized low density lipoprotein is mediated by distinct endothelial ligands, *Atherosclerosis* 136 (1998) 297–303, [https://doi.org/10.1016/s0021-9150\(97\)00223-2](https://doi.org/10.1016/s0021-9150(97)00223-2).
- [3] F. Yatian, D. Yanlin, Z. Jing, C. Song Lin, K.J.A.B. Bee Luan, Biofilms exacerbate atherogenesis through macrophage-induced inflammatory responses in a fibrous plaque microsystem model, *Acta Biomater.* (2023) 168, <https://doi.org/10.1016/j.actbio.2023.06.028>.
- [4] N. Kume, H. Moriwaki, H. Kataoka, M. Minami, T. Murase, T. Sawamura, T. Masaki, T. Kita, Inducible expression of LOX-1, a novel receptor for oxidized LDL in macrophages and vascular smooth muscle cells, *Ann. N. Y. Acad. Sci.* 902 (2006) 323–327, <https://doi.org/10.1111/j.1749-6632.2000.tb06332.x>.
- [5] A. Pirillo, G.D. Norata, A.L. Catapano, LOX-1, OxLDL, and atherosclerosis, *Mediat. Inflamm.* (2013) 1–12, <https://doi.org/10.1155/2013/152786>, 2013.
- [6] D.A. Chistiakov, Y.V. Bobryshev, N.G. Nikiforov, N.V. Elizova, I.A. Sobenin, A. N. Orekhov, RETRACTED: macrophage phenotypic plasticity in atherosclerosis: the associated features and the peculiarities of the expression of inflammatory genes, *Int. J. Cardiol.* 184 (2015) 436–445, <https://doi.org/10.1016/j.ijcard.2015.03.055>.
- [7] E. Favari, A. Chroni, U.J. Tietge, I. Zanotti, J.C. Escola-Gil, F. Bernini, Cholesterol efflux and reverse cholesterol transport, *Handb. Exp. Pharmacol.* 224 (2015) 181–206, [https://doi.org/10.1007/978-3-319-09665-0\\_4](https://doi.org/10.1007/978-3-319-09665-0_4).
- [8] C. Rebecca A, A. Dalia S, F. Jonathan J, P. Latrisha K, G. Carol R, U. Kathryn E, J. Laurie B, M.J.A.B. Prabhas V, Athero-inflammation nanotherapeutics: ferulic acid-based poly(anhydride-ester) nanoparticles attenuate foam cell formation by

- regulating macrophage lipogenesis and reactive oxygen species generation, *Acta Biomater.* (2017) 57, <https://doi.org/10.1016/j.actbio.2017.05.029>.
- [9] Z. Xu, S. Yufen, C. Fangjian, W. Sisi, G. Hu, W. Fan, Z. Lei, S.J.A.H.M. Zhen, Oxidized low-density lipoprotein (Ox-LDL)-Triggered double-lock probe for spatiotemporal lipoprotein oxidation and atherosclerotic plaque imaging, *Adv. Healthcare Mater.* 12 (2023), <https://doi.org/10.1002/adhm.202301595>.
- [10] A. Batista-Gonzalez, R. Vidal, A. Criollo, L.J. Carreño, New insights on the role of lipid metabolism in the metabolic reprogramming of macrophages, *Front. Immunol.* 10 (2020) 2993, <https://doi.org/10.3389/fimmu.2019.02993>.
- [11] A. Remmerie, C.L. Scott, Macrophages and lipid metabolism, *Cell. Immunol.* 330 (2018) 27–42, <https://doi.org/10.1016/j.cellimm.2018.01.020>.
- [12] M. Kaplan, A. Shur, Y. Tendler, M1 macrophages but not M2 macrophages are characterized by upregulation of CRP expression via activation of NFkB: a possible role for ox-LDL in macrophage polarization, *Inflammation* 41 (2018) 1477–1487, <https://doi.org/10.1007/s10753-018-0793-8>.
- [13] X. Zhou, X. Chen, L. Zhang, J. Yuan, H. Lin, M. Zhu, X. Xu, G. Dong, J. Fu, W. Wu, Mannose-binding lectin reduces oxidized low-density lipoprotein induced vascular endothelial cells injury by inhibiting LOX1-ox-LDL binding and modulating autophagy, *Biomedicines* (2023) 11, <https://doi.org/10.3390/biomedicines11061743>.
- [14] P.I. Mäkinen, J.P. Lappalainen, S.E. Heinonen, P. Leppanen, M.T. Lahteenluoma, J. V. Aarnio, J. Heikkilä, M.P. Turunen, S. Yla-Herttula, Silencing of either SR-A or CD36 reduces atherosclerosis in hyperlipidaemic mice and reveals reciprocal upregulation of these receptors, *Cardiovasc. Res.* 88 (2010) 530–538, <https://doi.org/10.1093/cvr/cvq235>.
- [15] G. Endemann, L. Stanton, K. Madden, C. Bryant, R. White, A.J. T.J.O. b. c. Protter, CD36 is a receptor for oxidized low density lipoprotein, *J. Biol. Chem.* 268 (1993) 11811–11816, [https://doi.org/10.1016/0021-5793\(94\)00877-9](https://doi.org/10.1016/0021-5793(94)00877-9).
- [16] A.G. Jay, A.N. Chen, M.A. Paz, J.P. Hung, J.A. Hamilton, CD36 binds oxidized low density lipoprotein (LDL) in a mechanism dependent upon fatty acid binding, *J. Biol. Chem.* 290 (2015) 4590–4603, <https://doi.org/10.1074/jbc.M114.627026>.
- [17] C.-H. Heldin, B. Lu, R. Evans, J.S. Gutkind, Signals and receptors, *Cold Spring Harbor Perspect. Biol.* 8 (2016) a005900, <https://doi.org/10.1101/cshperspect.a005900>.
- [18] L. Wang, H. Li, Y. Tang, P.J. F.i. e. Yao, Potential mechanisms and effects of efferocytosis in atherosclerosis, *Front. Endocrinol.* 11 (2020) 585285, <https://doi.org/10.3389/fendo.2020.585285>.
- [19] D. Green, T. Oguin, J.J. C.d. Martinez differentiation, The clearance of dying cells: table for two, *Cell Death Differ.* 23 (2016) 915–926, <https://doi.org/10.1038/cdd.2015.172>.
- [20] T. Yamao, T. Noguchi, O. Takeuchi, U. Nishiyama, H. Morita, T. Hagiwara, H. Akahori, T. Kato, K. Imagaki, H. Okazawa, Y. Hayashi, T. Matozaki, K. Takeda, S. Akira, M. Kasuga, Negative regulation of platelet clearance and of the macrophage phagocytic response by the transmembrane glycoprotein SHPS-1, *J. Biol. Chem.* 277 (2002) 39833–39839, <https://doi.org/10.1074/jbc.M03287200>.
- [21] B.R. Blazar, F.P. Lindberg, E. Ingulli, A. Panoskaltsis-Mortari, P.-A. Oldenborg, K. Iizuka, W.M. Yokoyama, P.A. Taylor, Cd47 (Integrin-Associated protein) engagement of dendritic cell and macrophage counterreceptors is required to prevent the clearance of donor lymphohematopoietic cells, *J. Exp. Med.* 194 (2001) 541–550, <https://doi.org/10.1084/jem.194.4.541>.
- [22] T. Ishikawa-Sekigami, Y. Kaneko, H. Okazawa, T. Tomizawa, J. Okajo, Y. Saito, C. Okuzawa, M. Sugawara-Yokoo, U. Nishiyama, H. Ohnishi, T. Matozaki, Y. Nojima, SHPS-1 promotes the survival of circulating erythrocytes through inhibition of phagocytosis by splenic macrophages, *Blood* 107 (2006) 341–348, <https://doi.org/10.1182/blood-2005-05-1896>.
- [23] P.-A. Oldenborg, A. Zheleznyak, Y.-F. Fang, C.F. Lagenaar, H.D. Gresham, F. P. Lindberg, Role of CD47 as a marker of self on red blood cells, *Science* 288 (2000) 2051–2054, <https://doi.org/10.1126/science.288.5473.2051>.
- [24] E. Eladl, R. Tremblay-LeMay, N. Rastgoo, R. Musani, W. Chen, A. Liu, H. Chang, Role of CD47 in hematological malignancies, *J. Hematol. Oncol.* 13 (2020) 96, <https://doi.org/10.1186/s13045-020-00930-1>.
- [25] W. Zhang, Q. Huang, W. Xiao, Y. Zhao, J. Pi, H. Xu, H. Zhao, J. Xu, C.E. Evans, H. Jin, Advances in anti-tumor treatments targeting the CD47/SIRP $\alpha$  Axis, *Front. Immunol.* 11 (2020) 18, <https://doi.org/10.3389/fimmu.2020.00018>.
- [26] L. Chen, Z. Zhou, C. Hu, M.F. Maitz, L. Yang, R. Luo, Y. Wang, Platelet membrane-coated nanocarriers targeting Plaques to deliver anti-CD47 antibody for atherosclerotic therapy, *Research (Wash D C)* 2022 (2022) 9845459, <https://doi.org/10.34133/2022/9845459>.
- [27] L. Yi, H. Qian, H. Mengyun, C. Tingting, C.J.A.B. Xia, A nano-bioconjugate modified with anti-SIRP $\alpha$  antibodies and antisense oligonucleotides of mTOR for anti-atherosclerosis therapy, *Acta Biomater.* (2024) 176, <https://doi.org/10.1016/j.actbio.2023.12.031>.
- [28] Y. Kojima, J. Volkmer, K. McKenna, M. Civelek, A. Lusis, C. Miller, D. Direnzo, V. Nanda, J. Ye, A. Connolly, E. Schadt, T. Quertermous, P. Betancur, L. Maegdefessel, L. Matic, U. Hedin, I. Weissman, N.J.N. Leeper, CD47-blocking antibodies restore phagocytosis and prevent atherosclerosis, *Nature* 536 (2016) 86–90, <https://doi.org/10.1038/nature18935>.
- [29] F. Liu, N. Ding, D. Huo, G. Yang, K. Wei, G. Guan, Y. Li, J. Yang, T. Wang, Y. Wang, J. Tan, W. Zeng, C. Zhu, Surface-engineered monocyte inhibits atherosclerotic plaque destabilization via graphene quantum dot-mediated MicroRNA delivery, *Adv. Healthcare Mater.* 8 (2019) e1900386, <https://doi.org/10.1002/adhm.201900386>.
- [30] T. Li, M. Morgan, S. Choksi, Y. Zhang, Y. Kim, Z.J. N.i. Liu, MicroRNAs modulate the noncanonical transcription factor NF-kappaB pathway by regulating expression of the kinase IKK $\alpha$  during macrophage differentiation, *Nat. Immunol.* 11 (2010) 799–805, <https://doi.org/10.1038/ni.1918>.
- [31] J. Johnnidis, M. Harris, R. Wheeler, S. Stehling-Sun, M. Lam, O. Kirak, T. Brummelkamp, M. Fleming, F.J.N. Camargo, Regulation of progenitor cell proliferation and granulocyte function by microRNA-223, *Nature* 451 (2008) 1125–1129, <https://doi.org/10.1038/nature06607>.
- [32] M.E.W. Logtenberg, F.A. Scheeren, T.N. Schumacher, The CD47-SIRP $\alpha$  immune checkpoint, *Immunity* 52 (2020) 742–752, <https://doi.org/10.1016/j.immuni.2020.04.011>.
- [33] Z. Caparevic, N. Kostic, S. Ilic, J. Radokovic, D. Marina, B. Pencic, I. Radokovic, Oxidized LDL and C-reactive protein level in relation to carotid intima-media thickness in population with risk factors for atherosclerosis, *Srp. Arh. Celok. Lek.* 137 (2009) 140–145, <https://doi.org/10.2298/sarh0904140c>.
- [34] D. Wang, Y. Yang, Y. Lei, N.T. Tzvetkov, X. Liu, A.W.K. Yeung, S. Xu, A. G. Atanasov, Q. Ma, Targeting foam cell formation in atherosclerosis: therapeutic potential of natural products, *Pharmacol. Rev.* 71 (2019) 596–670, <https://doi.org/10.1124/pr.118.017178>.
- [35] J.B. Johnnidis, M.H. Harris, R.T. Wheeler, S. Stehling-Sun, M.H. Lam, O. Kirak, T. R. Brummelkamp, M.D. Fleming, F.D. Camargo, Regulation of progenitor cell proliferation and granulocyte function by microRNA-223, *Nature* 451 (2008) 1125–1129, <https://doi.org/10.1038/nature06607>.
- [36] K. Hirose, K. Iwabuchi, K. Shimada, T. Kiyanagi, C. Iwahara, H. Nakayama, H. Daida, Different responses to oxidized low-density lipoproteins in human polarized macrophages, *Lipids Health Dis.* 10 (2011) 1, <https://doi.org/10.1186/1476-511x-10-1>.
- [37] Y. Qie, H. Yuan, C.A. von Roemeling, Y. Chen, X. Liu, K.D. Shih, J.A. Knight, H. W. Tun, R.E. Wharen, W. Jiang, B.Y.S. Kim, Surface modification of nanoparticles enables selective evasion of phagocytic clearance by distinct macrophage phenotypes, *Sci. Rep.* 6 (2016) 26269, <https://doi.org/10.1038/srep26269>.
- [38] D.A. Chistiakov, A.A. Melnichenko, V.A. Myasoedova, A.V. Grechko, A.N. Orekhov, Mechanisms of foam cell formation in atherosclerosis, *J. Mol. Med.* 95 (2017) 1153–1165, <https://doi.org/10.1007/s00109-017-1575-8>.
- [39] G. Mao, S.S. Smyth, A.J. Morris, Regulation of PLPP3 gene expression by NF- $\kappa$ B family transcription factors, *J. Biol. Chem.* 294 (2019) 14009–14019, <https://doi.org/10.1074/jbc.RA119.009002>.
- [40] W. Yang, J. Li, M. Zhang, H. Yu, Y. Zhuang, L. Zhao, L. Ren, J. Gong, H. Bi, L. Zeng, Y. Xue, J. Yang, Y. Zhao, S. Wang, S. Gao, Z. Fu, D. Li, J. Zhang, T. Wang, M. Shan, B. Tang, X. Li, Elevated expression of the rhythm gene NFIL3 promotes the progression of TNBC by activating NF- $\kappa$ B signaling through suppression of NFKBIA transcription, *J. Exp. Clin. Cancer Res.* 41 (2022) 67, <https://doi.org/10.1186/s13046-022-02260-1>.
- [41] R.T. Robinson, IL12R $\beta$ 1: the cytokine receptor that we used to know, *Cytokine* 71 (2015) 348–359, <https://doi.org/10.1016/j.cyto.2014.11.018>.
- [42] N. Mukaida, S.I. Sasaki, T. Baba, CCL4 signaling in the tumor microenvironment, *Adv. Exp. Med. Biol.* 1231 (2020) 23–32, [https://doi.org/10.1007/978-3-030-36674-3\\_3](https://doi.org/10.1007/978-3-030-36674-3_3).
- [43] T. Tanaka, M. Narazaki, K. Masuda, T. Kishimoto, Regulation of IL-6 in immunity and diseases, *Adv. Exp. Med. Biol.* 941 (2016) 79–88, [https://doi.org/10.1007/978-94-024-0921-5\\_4](https://doi.org/10.1007/978-94-024-0921-5_4).
- [44] M.A. Howlader, E.P. Demina, S. Samarani, T. Guo, A. Caillon, A. Ahmad, A. V. Pshezhetsky, C.W. Cairo, The Janus-like role of neuraminidase isoenzymes in inflammation, *Faseb J.* 36 (2022) e22285, <https://doi.org/10.1096/fj.202101218R>.
- [45] D.A. Chistiakov, Y.V. Bobryshev, A.N. Orekhov, Macrophage-mediated cholesterol handling in atherosclerosis, *J. Cell Mol. Med.* 20 (2015) 17–28, <https://doi.org/10.1111/jcmm.12689>.
- [46] J. Lappalainen, N. Yeung, S.D. Nguyen, M. Jauhainen, P.T. Kovanen, M. Lee-Rueckert, Cholesterol loading suppresses the atheroinflammatory gene polarization of human macrophages induced by colony stimulating factors, *Sci. Rep.* 11 (2021) 4923, <https://doi.org/10.1038/s41598-021-84249-y>.
- [47] V.N. Sukhorukov, V.A. Khotina, Y.S. Chegodaev, E. Ivanova, I.A. Sobenin, A. N. Orekhov, Lipid metabolism in macrophages: focus on atherosclerosis, *Biomedicines* 8 (2020), <https://doi.org/10.3390/biomedicines8080262>.
- [48] F. Liu, Y. Mao, J. Yan, Y. Sun, Z. Xie, F. Li, F. Yan, H. Zhang, P. Zhang, Bionic microbubble neutrophil composite for inflammation-responsive atherosclerotic vulnerable plaque pluripotent intervention, *Research (Wash D C)* 2022 (2022) 9830627, <https://doi.org/10.34133/2022/9830627>.
- [49] A.K. Hubbard, R. Rothlein, Intercellular adhesion molecule-1 (ICAM-1) expression and cell signaling cascades, *Free Radic. Biol. Med.* 28 (2000) 1379–1386, [https://doi.org/10.1016/s0891-5849\(00\)00223-9](https://doi.org/10.1016/s0891-5849(00)00223-9).
- [50] S. Potteaux, E.L. Gautier, S.B. Hutchison, N. van Rooijen, D.J. Rader, M.J. Thomas, M.G. Sorci-Thomas, G.J. Randolph, Suppressed monocyte recruitment drives macrophage removal from atherosclerotic plaques of Apoe $^{-/-}$  mice during disease regression, *J. Clin. Invest.* 121 (2011) 2025–2036, <https://doi.org/10.1172/jci43802>.
- [51] B. Schieffer, M. Luchtefeld, Emerging role of chemokine receptor 7 in atherosclerosis, *trends in cardiovascular Medicine* 21 (2011) 211–216, <https://doi.org/10.1016/j.tcm.2012.05.012>.
- [52] M. Luchtefeld, C. Grothusen, A. Gagalick, K. Jagavelu, H. Schuett, U.J.F. Tietge, O. Pabst, K. Grote, H. Drexler, R. Förster, B. Schieffer, Chemokine receptor 7 knockout attenuates atherosclerotic plaque development, *Circulation* 122 (2010) 1621–1628, <https://doi.org/10.1161/circulationaha.110.956730>.
- [53] D. Kobayashi, M. Endo, H. Ochi, H. Hojo, M. Miyasaka, H. Hayasaka, Regulation of CCR7-dependent cell migration through CCR7 homodimer formation, *Sci. Rep.* 7 (2017) 8536, <https://doi.org/10.1038/s41598-017-09113-4>.

- [54] H. Kang, X. Li, K. Xiong, Z. Song, J. Tian, Y. Wen, A. Sun, X. Deng, V. Garcia, The entry and egress of monocytes in atherosclerosis: a biochemical and biomechanical driven process, *Cardiovascular Therapeutics* (2021) 1–17, <https://doi.org/10.1155/2021/6642927>, 2021.
- [55] K. Malekmohammad, E.E. Bezsonov, M. Rafieian-Kopaei, Role of lipid accumulation and inflammation in atherosclerosis: focus on molecular and cellular mechanisms, *Frontiers in Cardiovascular Medicine* 8 (2021) 707529, <https://doi.org/10.3389/fcvm.2021.707529>.
- [56] M. Gaggini, F. Gorini, C. Vassalle, Lipids in atherosclerosis: pathophysiology and the role of calculated lipid indices in assessing cardiovascular risk in patients with hyperlipidemia, *Int. J. Mol. Sci.* 24 (2023), <https://doi.org/10.3390/ijms24010075>.
- [57] Y.V. Bobryshev, Monocyte recruitment and foam cell formation in atherosclerosis, *Micron* 37 (2006) 208–222, <https://doi.org/10.1016/j.micron.2005.10.007>.
- [58] S.L. Deshmane, S. Kremlév, S. Amini, B.E. Sawaya, Monocyte chemoattractant protein-1 (MCP-1): an overview, *J. Interferon Cytokine Res.* 29 (2009) 313–326, <https://doi.org/10.1089/jir.2008.0027>.
- [59] P.W. Fok, Growth of necrotic cores in atherosclerotic plaque, *Math. Med. Biol.* 29 (2011) 301–327, <https://doi.org/10.1093/imammb/dqr012>.
- [60] J.A. Lardizabal, P. Deedwania, Lipid-lowering therapy with statins for the primary and secondary prevention of cardiovascular disease, *Cardiol. Clin.* 29 (2011) 87–103, <https://doi.org/10.1016/j.ccl.2010.10.002>.
- [61] J.E. McLaren, D.R. Michael, T.G. Ashlin, D.P. Ramji, Cytokines, macrophage lipid metabolism and foam cells: implications for cardiovascular disease therapy, *Prog. Lipid Res.* 50 (2011) 331–347, <https://doi.org/10.1016/j.plipres.2011.04.002>.
- [62] L. Jin, Y. Li, Structural and functional insights into nuclear receptor signaling, *Adv. Drug Deliv. Rev.* 62 (2010) 1218–1226, <https://doi.org/10.1016/j.adrev.2010.08.007>.
- [63] A. Christofides, E. Konstantinidou, C. Jani, V.A. Boussiotis, The role of peroxisome proliferator-activated receptors (PPAR) in immune responses, *Metabolism* 114 (2021) 154338, <https://doi.org/10.1016/j.metabol.2020.154338>.
- [64] M.B. Fessler, The challenges and promise of targeting the Liver X Receptors for treatment of inflammatory disease, *Pharmacol. Therapeut.* 181 (2018) 1–12, <https://doi.org/10.1016/j.pharmthera.2017.07.010>.
- [65] Y. Zhu, Y. Li, Liver X Receptors as potential therapeutic targets in atherosclerosis, *Clin. Invest. Med.* 32 (2009) E383–E394, <https://doi.org/10.25011/cim.v32i5.6927>.
- [66] F. Fei, X. Crystal, L. Chunli, L. Xiaoheng, L.J.R.B. Song, Tuning macrophages for atherosclerosis treatment, *Regen Biomater.* (2023) 10, <https://doi.org/10.1093/rb/rbac103>.
- [67] Y. Azuma, H. Nakagawa, K. Dote, K. Higai, K.J.B. Matsumoto, p. bulletin, Decreases in CD31 and CD47 levels on the cell surface during etoposide-induced Jurkat cell apoptosis, *Biol. Pharm. Bull.* 34 (2011) 1828–1834, <https://doi.org/10.1248/bpb.34.1828>.
- [68] J. Yan, T. Horng, Lipid metabolism in regulation of macrophage functions, *Trends Cell Biol.* 30 (2020) 979–989, <https://doi.org/10.1016/j.tcb.2020.09.006>.
- [69] V. Evros, F.-P.J.I.J.M.S. Renalison, Impact of lipid metabolism on macrophage polarization: implications for inflammation and tumor immunity, *Int. J. Mol. Sci.* 24 (2023), <https://doi.org/10.3390/ijms241512032>.
- [70] M. Nataliya V, N. Nikita G, M. Alexandra A, K. Vladislav, S. Nikolay K, O. Varvara A, O.J.B. Alexander N, Functional phenotypes of intraplaque macrophages and their distinct roles in atherosclerosis development and athero-inflammation, *Biomedicines* 10 (2022), <https://doi.org/10.3390/biomedicines10020452>.
- [71] L. Ping, J. Hong-Hai, L. Yan-Jie, G.J.F.M.B. Shou-Dong, Macrophage plasticity and atherosclerosis therapy, *Front. Mol. Biosci.* (2021) 8, <https://doi.org/10.3389/fmbo.2021.679797>.
- [72] U.J. I.j. o. t. r. Das, Atherosclerosis and prostaglandins, *Int. J. Tissue React.* 4 (1982) 127–132.
- [73] M. Bäck, C. Weber, E. Lutgens, Regulation of atherosclerotic plaque inflammation, *J. Intern. Med.* 278 (2015) 462–482, <https://doi.org/10.1111/joim.12367>.
- [74] Z. Mallat, C. Heymes, J. Ohan, E. Faggin, G. Lesèche, A. Tedgui, Expression of interleukin-10 in advanced human atherosclerotic plaques, *Arterioscler. Thromb. Vasc. Biol.* 19 (1999) 611–616, <https://doi.org/10.1161/01.ATV.19.3.611>.
- [75] K. Zhang, X.-z. Huang, X.-n. Li, M. Feng, L. Li, X.-j. Cai, C. Zhang, X.-l. Liu, M.-x. Zhang, Y. Zhang, X.-l. Wang, M. Zhang, Interleukin 6 destabilizes atherosclerotic plaques by downregulating prolyl-4-hydroxylase α1 via a mitogen-activated protein kinase and c-Jun pathway, *Arch. Biochem. Biophys.* 528 (2012) 127–133, <https://doi.org/10.1016/j.abb.2012.09.007>.
- [76] I. Brochériou, D. Stengel, L. Mattsson-Hultén, J. Stankova, M. Rola-Pleszczynski, F. Koskas, O. Wiklund, Y. Le Charpentier, E. Ninio, Expression of platelet-activating factor receptor in human carotid atherosclerotic plaques, *Circulation* 102 (2000) 2569–2575, <https://doi.org/10.1161/01.Cir.102.21.2569>.
- [77] D. Thiagarajan, N. Quadri, S. Jawahar, H. Zirpoli, C.H. del Pozo, R. López-Díez, S. N. Hasan, G. Yepuri, P.F. Gugger, B.S. Finlin, P.A. Kern, K. Gabbay, A.M. Schmidt, R. Ramasamy, Aldose reductase promotes diet-induced obesity via induction of senescence in subcutaneous adipose tissue, *Obesity* 30 (2022) 1647–1658, <https://doi.org/10.1002/oby.23496>.
- [78] C.-C. Key, A.C. Bishop, X. Wang, Q. Zhao, G.-y. Chen, M.A. Quinn, X. Zhu, Q. Zhang, J.S. Parks, Human G6PD3 overexpression promotes liver steatosis by increasing lysophosphatidic acid production and fatty acid uptake, *JLR (J. Lipid Res.)* 61 (2020) 1075–1086, <https://doi.org/10.1194/jlr.RA120000760>.
- [79] K.L. Houseknecht, B.M. Cole, P.J. Steele, Peroxisome proliferator-activated receptor gamma (PPAR $\gamma$ ) and its ligands: a review, *Domest. Anim. Endocrinol.* 22 (2002) 1–23, [https://doi.org/10.1016/s0739-7240\(01\)00117-5](https://doi.org/10.1016/s0739-7240(01)00117-5).
- [80] S. Mal, A.R. Dwivedi, V. Kumar, N. Kumar, B. Kumar, V. Kumar, Role of peroxisome proliferator-activated receptor gamma (PPAR $\gamma$ ) in different disease states: recent updates, *Curr. Med. Chem.* 28 (2021) 3193–3215, <https://doi.org/10.2174/092986732766200716113136>.
- [81] R. Bertolio, F. Napoletano, M. Mano, S. Maurer-Stroh, M. Fantuz, A. Zannini, S. Biccato, G. Sorrentino, G. Del Sal, Sterol regulatory element binding protein 1 couples mechanical cues and lipid metabolism, *Nat. Commun.* 10 (2019) 1326, <https://doi.org/10.1038/s41467-019-09152-7>.
- [82] F.O. Martínez, L. Helming, S. Gordon, Alternative activation of macrophages: an immunologic functional perspective, *Annu. Rev. Immunol.* 27 (2009) 451–483, <https://doi.org/10.1146/annurev.immunol.021908.132532>.
- [83] A. Oeckinghaus, S.J.C.S.H.P.B. Ghosh, The NF- $\kappa$ B family of transcription factors and its regulation, *Cold Spring Harbor Perspect. Biol.* 1 (2009) a000034, <https://doi.org/10.1101/cshperspect.a000034>.
- [84] S.C.J.N.R.I. Sun, The non-canonical NF- $\kappa$ B pathway in immunity and inflammation, *Nat. Rev. Immunol.* 17 (2017) 545, <https://doi.org/10.1038/nri.2017.52>.
- [85] R. Kleemann, S. Zadelaar, T. Kooistra, Cytokines and atherosclerosis: a comprehensive review of studies in mice, *Cardiovasc. Res.* 79 (2008) 360–376, <https://doi.org/10.1093/cvr/cvn120>.
- [86] H. Kan, K. Zhang, A. Mao, L. Geng, M. Gao, L. Feng, Q. You, X. Ma, Single-cell transcriptome analysis reveals cellular heterogeneity in the ascending aortas of normal and high-fat diet-fed mice, *Exp. Mol. Med.* 53 (2021) 1379–1389, <https://doi.org/10.1038/s12276-021-00671-2>.
- [87] R.J. Petrovan, A.S. Black, J. Bulgrien, D.J. Bonnet, L.K. Curtiss, in: *Conference on Arteriosclerosis*, 2007.